Durability Evaluation of Cement-based Repair Materials Used for Corrosion-damaged Steel-reinforced Concrete Structures

by

Boyu Wang
MASc, University of Victoria, 2018

A Thesis Submitted in Partial Fulfillment
of the Requirements for the Degree of

MASTER OF APPLIED SCIENCE

in the Department of Mechanical Engineering

Supervisory Committee

Durability Evaluation of Cement-based Repair Materials Used for Corrosion-damaged Steel-reinforced Concrete Structures

by

Boyu Wang
MASc, University of Victoria, 2018

Supervisory Committee

Rishi Gupta, Department of Civil Engineering
Supervisor

Caterina Valeo, Department of Mechanical Engineering
Departmental Member

Abstract

Concrete repair materials are being widely used to restore and extend the service life of structures. While most cement-based repair materials are compatible with concrete structures, their durability properties do not attract much attention which it deserves from researchers. Since repair materials can deteriorate like conventional concrete, the search for reliable, long-lasting concrete repair materials is becoming more intensive. Amongst other factors, concrete permeability and chloride diffusivity within concrete are believed to play a major role in determining the durability and success of the repair. These two parameters determine the penetration rate of aggressive substances into concrete and how fast degradation could take place. A number of test methods have been proposed to study these two factors, and the commonly used test methods are water penetration, surface/bulk electrical resistivity, rapid chloride permeability (RCP), and half-cell potential. However, the relationship between each durability test method and their correlation with compressive strength measurement have not been fully understood. So, in this study, we aim for using multiple testing techniques, destructive and non-destructive, to evaluate the durability of concrete repair materials as well as correlating different test methods.

Three types of commercially available cement-based materials are tested and evaluated, and results have indicated that cementitious concrete mortar (termed as Mix M) amongst others has the best durability performance which means low water permeability, high resistivity, and compressive strength. Whereas, the flexural performance of Mix M still needs some improvement in terms of flexural strength and flexural toughness. For various durability testing methods, surface resistivity is found to have a strong linear relation and a polynomial relation to bulk resistivity and water permeability respectively. No relationship is established between concrete resistivity and compressive strength, though high-strength concrete tends to have a high resistivity in our study. RCP test results do not correlate well with resistivity measurements, which requires further study to overcome its heating and binding effect when measurements are being taken. Half-cell potential method is used for validating test results but it reveals no difference for materials with different permeability and resistivity.

A model is proposed to counteract temperature's effect while calculating the coefficient of diffusion, which indicates the concrete to resist chloride diffusion. It is found that this model can

shift the RCP measurement slightly closer to its theoretical prediction but the difference between them is still large. Therefore, further research is required for acquiring more raw data from RCP measurements as the regression analysis input. In addition, a more comprehensive model that involves more correction factors for binding effects, etc., is also needed.

Supervisory Committee

Rishi Gupta, Department of Civil Engineering
Supervisor

Caterina Valeo, Department of Mechanical Engineering
Departmental Member

Table of Contents

List of Tables

List of Figures

List of Acronyms

RCP	Rapid Chloride Permeability
DIN	Deutsches Institut für Normung e.V., German Institute for Standardization
RFT	Radial flow through
DC	Direct current
AASHTO	American Association of State Highway and Transportation Officials
ASTM	American Society for Testing and Materials
AC	Alternating current
CM	Cementitious Material
SR	Surface resistivity
BR	Bulk resistivity
WP	Water penetration
Comp	Compression
HC	Half cell
MTI	Measurement Technology Inc.
DAQ	Data acquisition
SSD	Surface saturated dry
SEM	Scanning electron microscope
EDX	Energy-dispersive X-ray spectroscopy
ITZ	Interfacial Transition Zone

Acknowledgments

Firstly, I would like to greatly thank my mentor and supervisor, Dr. Rishi Gupta, for his guidance throughout my Master's journey. I am grateful for not only the knowledge he imparted me, but the working attitude he showed me as being an excellent civil engineer. I feel proud to be one of your students and lucky to work with you.

Also, I would like to thank my colleges, Pejman Azarsa, Harsh Rathod, and Ridhi Vora, for giving me a lot of great advice and support for my project.

I am immensely thankful for Civil Engineering Technical Support, Dr. Armando Tura and Mr. Matthew Walker for their dedicated assistance in conducting multiple experiments.

I would like to thank all my friends and colleagues of the Faculty of Engineering and the Civil Research Group.

Dedication

This thesis is dedicated to my parents, who have given me unconditional love and support, and inspire me to explore the science world. Thanks to my girl friend, who encourages me to pursue my dreams and go through difficult time with me. Also, I want to express great thanks to my cousin in Montreal for continuously mental support.

Chapter 1 Introduction

1.1 Overview

Concrete is one of the most widely used building materials around the world. Numerous civil structures and bridges are built using concrete. Similar to many other artifacts, concrete structures face the problem of aging and deterioration when reaching the end of their life cycles. Aging infrastructure burdens the Canadian Economy. According to Canadian Infrastructure Report 2016, the reinvestment rate of bridges is at 0.80%, which is about $165 million. This figure falls short from the target of 1.0% to 1.7% signifying the conditions of bridges will be in decline at the current rate [1]. In addition, structurally deficient infrastructure poses a serious safety risk to the general public, so it is crucial to focus on the development of concrete repair and durability test methods in order to keep up with the increasing number of aging structures. Reinforced concrete structures are subjected to degradation by factors such as traffic load, freeze-thaw cycles, and chloride ingression from de-icing salt and high salt content in the air near marine environments. When the steel reinforcements underneath the concrete deck lose the passive layer and corrosion begins to occur, the expansion of the corrosion product causes additional stress on the concrete and crack initiation might occur as a consequence.

Due to the deterioration of the concrete structure, repair materials are employed to retain and extend the service life of structures. So far, there are literally hundreds of different types of repair materials, some of which are commercially available but some are not. In general, most of the commonly used repair materials are formulated with cement, polymer or both [2]. Despite the widespread use of concrete repair, a lack of comprehensive understanding of the properties of the repair materials and suitable guidelines poses some obstacles to their applications. Just like conventional concrete, concrete repair material can deteriorate due to the environmental conditions, compatibility with the substrate, and the penetration of aggressive chemicals (chloride ions). It is believed that various factors can impede the improvements of the durability of concrete repairs, including insufficient condition evaluation for corrosion, lack of construction practices and quality control, and the choice of repair materials [3]. Hence, it is worth to firstly know how to achieve a long-lasting repair, and what factors can influence the effectiveness of repair work.

Longevity of the repair work was considered a function of the intrinsic durability of the materials and long-term bonding strength with the substrate [4]. The bonding strength can be affected by the chemical, electrochemical, permeability, and dimensional compatibility, such as thermal expansion, elastic modulus, etc., between repair work and the substrate [4]–[6], as demonstrated in Fig. 1. Although there is no widely accepted rubric for selecting concrete repair, there are several factors that people usually consider including exposure conditions, compatibility to substrate, durability, structural and functional requirements [7]–[9].

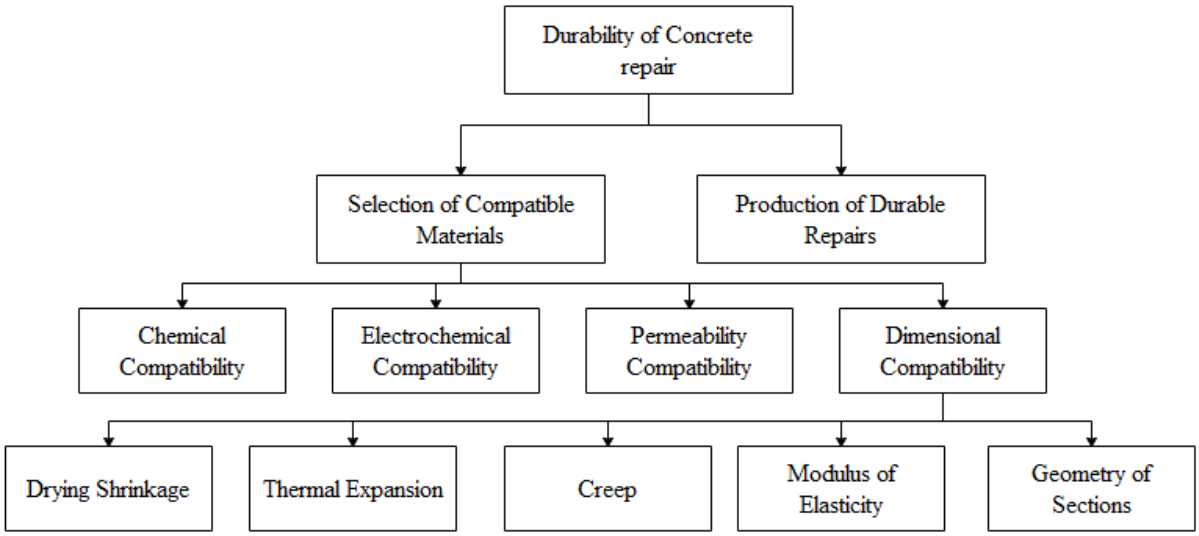

Figure 1 Factors affecting the durability of concrete repair **[5]**

It is obvious that not only one factor can define concrete durability considering concrete corrosion is a complex process. Apart from permeability and mechanical properties, there is a lack of more comprehensive investigations into other aspects such as diffusivity and electrical resistance of repair materials. So, in order to select the proper aspects to study, it is of great importance to first understand the main corrosion mechanisms of concrete.

The degradation of concrete repair was found to result from four main mechanisms including freeze/thaw cycle, alkali-aggregate reaction, chemical attack to the surface, and rebar corrosion due to chloride ingress. All these mechanisms are controlled by three principle transport mechanisms which include diffusion, permeation and capillary suction [4], [10]. These three processes determine the penetration rate of aggressive materials and how fast degradation

phenomena could take place [11]. If a hydraulic water head is applied on one surface of the concrete and some aggressive ions are present, they can easily permeate into the concrete with the help of water pressure. Highly permeable concrete makes it easier for ions, such as chloride ions, to come in contact with reinforcement rebars and cause corrosion. The permeability of concrete can be characterized using the water penetration method, which is one of the most widely used test methods for permeability assessment, and it has been standardized as DIN1048 [12].

Capillary suction will take place when concrete undergoes wetting and drying cycles. As a concrete wet surface is exposed to water, the substance dissolved in water will be sucked into the pore structure by means of the capillary force [10].

The diffusion is a process by which liquids, gases, or ions are transported through a porous material due to the concentration gradient. This is the main transport mechanism for concrete structures when it is exposed to salt water in marine environments [13]. Rapid chloride permeability test method (RCP) has long been used for evaluating diffusivity of chloride ions in concrete. Since RCPT has several drawbacks such as the heating effect, some researchers have suggested measuring concrete resistance using surface/bulk electrical resistivity technique as a replacement [14], [15].

1.2 Proposed work

The aim of this work is to investigate the durability performance of three types of commercially available repair materials in marine applications. Since capillary suction only exists in some special cases (wetting and drying cycle), and it can only result in chloride penetration at the concrete surface, permeability and diffusivity properties of repair materials are the focus in this study. Additionally, for the sake of simulating the marine environment experienced by concrete repairs, a 3.5% wt sodium chloride solution is used to immerse our specimens in order to study its effect. As mentioned before, the water penetration test will be used to study permeability. Additionally, RCP and surface/bulk resistivity tests will be conducted on repair materials to study diffusivity properties. Mechanical properties of our repair mixes will also be evaluated and their correlation with the aforementioned testing techniques will be established. Lastly, the half-cell potential test,

which is used to assess the state of corrosion for rebars, will be performed on the same type of materials to validate the foregoing test results.

In the following sections, different testing techniques for evaluating concrete durability, such as permeability and diffusivity, will be reviewed as well as their correlation analysis conducted by previous researchers. Also, a brief introduction to the repair materials and its classification are explained. Then, the experimental investigation will be introduced including sample casting, specimen preparation, as well as the experimental testing sections. After that, results from various test methods are analyzed and discussed followed by a conclusion from these discussions. Lastly, recommendations for future work will be proposed based on the conclusions.

Chapter 2 Background and literature review

2.1 Corrosion of reinforcement

The corrosion of reinforcing steel in concrete has been considered a major problem in civil engineering practice for many decades. It is known that steel corrosion is mainly attributed to the carbonation reaction and chloride attack, which can break down the passive layer formed on the steel surface and expose the unprotected rebars [7]. Carbonation reaction takes place as carbon dioxide along with moisture enter the pore network of concrete and neutralize the alkalinity of pore solutions.

As the carbonation transports through the concrete, pH values around reinforced steel gradually decrease until it reaches the threshold which indicates the onset of steel bar corrosion. Unlike carbonation, the mechanism of chloride-induced corrosion is somewhat different. The chloride ions, which serves as a catalyst, can contribute to the dissolution of passive layers even when there is no apparent pH drop [16].

Many researchers have studied the chloride transport in concrete. It is widely believed that chloride transport starts with capillary suction at near-surface locations especially when the surface is dry [7]. This process is followed by the chloride diffusion as a result of concentration gradients along the concrete depth, which is governed by Fick's second law and will be detailed in the following section.

2.2 Water permeability

The measurement of permeability is an important subject for structural health monitoring purposes. Permeability testing methodology can be classified into direct and indirect approaches concerning its theoretical basis [11]. The direct testing method is based on Darcy's law or its modified expression which uses the steady-state assumption [17]. According to Darcy's law which was discovered by Henry Darcy in the nineteenth century, the internal flow rate of a porous medium is directly proportional to the pressure gradient of the material. And a parameter, defined as the

coefficient of permeability, is derived from Darcy's law to quantify the water permeability of concrete materials. For direct permeability testing, Darcy's Law is the theoretical basis according to which, water flux in pore networks is equal to the product of the coefficient of permeability and pressure gradient. Darcy's Law can be written in Eq. 1 and Eq. 2 as shown below [18], [19].

$$\mathbf{J} = -\frac{k}{\eta}\nabla P \tag{1}$$

$$\mathrm{J} = k_w \nabla h = -\left(\frac{k\rho g}{\eta}\right)\nabla h \tag{2}$$

where, J is the water flux of the flow, k_w is the coefficient of permeability, P is the exterior pressure applied, η represents the dynamic viscosity, h is the water head, g represents the gravitational acceleration, ρ indicates the fluid density. The coefficient of permeability k_w is expressed as a product of coefficient k and the fluid properties, as well as the gravitational acceleration.

In contrast, instead of measuring flow rate to calculate permeability directly, material properties, such as surface resistivity and elastic modulus, are used to correlate with concrete permeability characteristics. Compared with direct methods, indirect methods often take less time and have the capability to measure very low permeability [11].

The direct method evaluates permeability by measuring the flow rate through the porous material under a pressure gradient. The testing apparatus for the direct method is relatively simple and easy to be performed. However, testing process of direct method is usually time-consuming due to the steady-state assumption, which means the flow rate does not change with time when measurements are being taken, and thus it usually takes several days or weeks to make measurements. In contrast, indirect testing techniques can cut down testing time to minutes or hours by correlating permeability to other material properties. Table 1 reviews some commonly used direct and indirect methods for measuring permeability and their characteristics.

Table 1 Direct and indirect permeability test methods

	Method and principle	Application and advantage	Limitations
Direct method	**Water penetration test** – correlate permeability with water penetration depth	Simple testing apparatus; easy to interpret test results	Steady-state flow condition is hard to attain [20]
	Radial flow through test (RFT) – Pressurize water into hollow cylindrical samples and calculate permeability based on internal fluid level	Good repeatability; low potential leakage; High accuracy due to large contact area	Samples need to be fully saturated with water; Sample preparation is difficult [21], [22]
	Centrifuge technique – calculate the coefficient of permeability by measuring steady-state unsaturated flow in a centrifugal field	Applicable for materials whose permeability ranges from 10^{-6} to 10^{-13} m/s; Easy to adjust by simply changing the speed of rotation	The sample can be damaged if rotational speed is too high [11], [23]
	High-pressure triaxial cell – Correlate water inlet and outlet with confining pressure to calculate permeability	Capable of measuring the permeability of high-performance and high-strength concrete; Variability of replicate results is low	High pressure may introduce artificial cracks [24], [25]
Indirect method	**Dynamic pressurization** (**hollow/solid**)– correlate permeability with concrete cylinder expansion under hydraulic pressure	Short testing time; applicable for both high and low permeability samples	Test method for solid cylinders is not suitable for specimens with high permeability [11], [26]
	Beam bending test – Permeability is a function of the rate of change of the forces that sustain the deflection of the beam	Permeability can be measured in a few hours; high pressure is not needed during the test; water leakage does not affect results	Difficult to perform due to the risk of creating cracks during bending test [27], [28]
	Thermal expansion kinetics – Correlate permeability with elastic modulus of the network, the compressibility of the liquid, and the difference between the thermal expansion coefficients of the solid and liquid phases when the concrete is heated	Particularly applicable for measuring very low permeability; can avoid the problems of leakage	Not suitable for materials whose full saturation state is hard to obtain [29], [30]

2.3 Rapid chloride permeability

For measuring the chloride ion penetrability of the concrete, there are multiple methods that have been widely used such as RCP test, surface/bulk resistivity test, and 90-day salt ponding test. The underlying theory of chloride diffusion is Fick's Law according to which one-dimensional chloride penetration can be expressed as:

$$J = -D_{eff} \frac{dC}{dx} \tag{3}$$

$$\frac{\partial C}{\partial t} = D_{eff} \frac{\partial^2 C}{\partial x^2} \tag{4}$$

where,

J = flux of chloride ions

D_{eff} = effective diffusion coefficient

C = concentration of chloride ions

x = longitudinal distance

Fick's first law shown in Eq.3 is applied in the context of steady-state conditions in which the chloride ion concentration is constant. Fick's second law as shown in Eq.4 is used for non-steady conditions when concentrations are changing.

In the 1970s, Whiting [31] first introduced the RCP method which monitors the electrical current passed through a concrete specimen over 6 hours when a 60 volt DC potential is maintained across the specimen. The total electrical charge was calculated and used as an indicator of concrete specimens to resist chloride ion ingress. This method was adopted by AASHTO in 1983 as T277 and by ASTM in 1991 as ASTM C1202 [32]. However, RCP method was mostly criticized for its heating effect due to high voltage imposed on the specimen, which results in misleading high electrical charge [33]. In addition, the involvement of some chemicals such as calcium nitrite can also cause higher coulomb values. Long-term chloride ponding test has shown that concrete mixes with and without calcium nitrite had the same resistance to chloride ion penetration [32].

2.4 Surface/Bulk electrical resistivity

Due to the limitations of the RCP test method, surface/bulk resistivity test methods were implemented to quantify the conductive properties of concrete materials and were regarded as an

alternative to RCP test [15], [34]. Bulk electrical resistivity technique applies an AC current between two end surfaces of the specimen through two metal plates and measures the potential drop between them. The electrical resistance of concrete specimens can be evaluated by dividing the measured voltage drop by the electrical current applied. Test mechanism is demonstrated in Fig. 2 and Eq. 5 is used to calculate specimen resistivity based on test results.

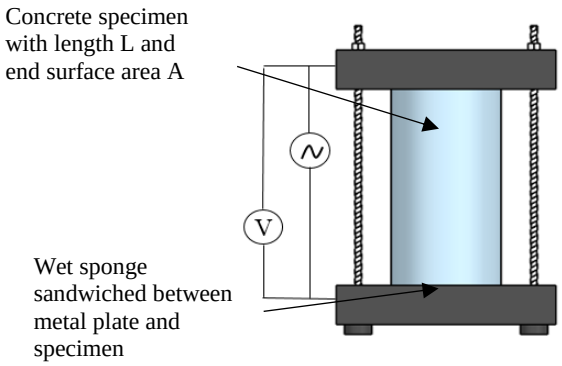

Figure 2 Bulk electrical resistivity schematic

$$\rho = \frac{A \cdot V_{bulk}}{L_{bulk} \cdot I_{bulk}} \tag{5}$$

where, I_{bulk} and V_{bulk} are the measured electrical current and voltage applied respectively; ρ indicates concrete resistivity; A represents the cross-sectional area and L indicates concrete specimen length.

Similarly, the surface electrical resistance of concrete is measured by means of the four-point Wenner probe, whose schematic is shown in Fig. 3. The four electrodes, which were pressed against the concrete surface, are straightly aligned and have equal spaces. The two exterior electrodes serve to generate an AC current while the inner two probes measure the corresponding voltage drop. The resistance value can be calculated following the same principle as bulk resistivity technique and by multiplying a geometry factor, the resistivity value can be acquired. Eq. 6 shows the formula for surface electrical resistivity calculation. Compared to RCP test, surface/bulk resistivity technique has advantages including easier sample preparation procedure, short testing time, low cost and variability [14], [15].

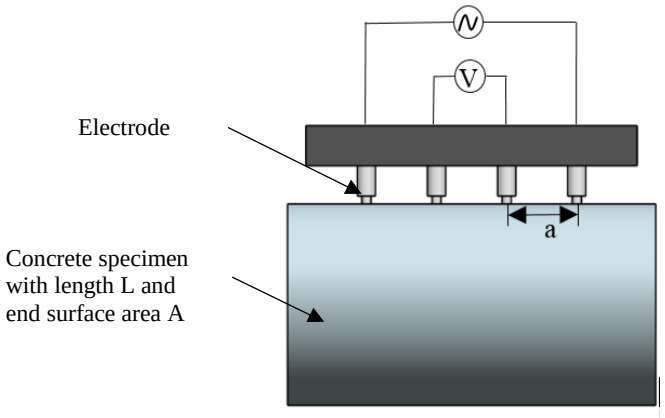

Figure 3 Surface resistivity test schematic

$$\rho = 2\pi a \cdot \frac{V_{surf}}{I_{surf}} \tag{6}$$

where, I_{surf} and V_{surf} are the measured electrical current and applied voltage, respectively; ρ indicates concrete resistivity; *a* is the distance between the probes.

2.5 Concrete repair materials

Most of the concrete repair materials can be classified either as cement-based or polymer-based concrete materials [35], [36]. For cement-based materials, cement is the main constituent which may be impregnated with polymer, silica-fume, fly-ash or any other materials as admixtures. In addition, some researchers subcategorize cement-based concrete into cementitious concrete and polymer modified concrete materials due to the fact that polymer as an admixture is widely used in repair materials [8], [37]. The polymer in concrete serves as a water reducer to produce a compound with good workability and lower shrinkage at lower water cement ratios. For polymer-based repair materials [38], [39], the polymer binder, which is in place of cement mortar, hold all the aggregates together. Use of polymers has advantages of fast curing, good freezing-and-thawing resistance, and good adhesion to most surfaces over conventional concrete. Table 2 summarizes several aspects compared between cementitious and polymer-added concrete repair materials.

However, only a few researchers have investigated and reported the intrinsic durability of repair materials. Cabrera and Al-Hasan [40] studied the compressive strength, bond strength, porosity

and permeability of four types of repair materials, two commercially available and two laboratory prepared materials. Their results showed that pozzolanic concrete mix seemed to show low porosity and oxygen permeability, which indicates good durability. Mangat and Limbachiya [41] investigated the water permeability, drying shrinkage and swelling, and strength properties of three commercially available generic repair materials. One of the important findings was that the presence of polymers in repair material can aid in reducing its water permeability and thus, promote its durability. Ueda et al. [42] evaluated the water permeability and bonding strength of cement-based repair materials and their results indicated that the resistance to water permeation was smaller along the interface between concrete and the repair material. From previous review, we can see that permeability was regarded as an important factor, and porosity, bond strength, mechanical properties, and effect of polymer addition are also related to durability of the concrete repair materials.

Table 2 Comparison between cementitious and polymer-added repair materials **[37]**

	Cementitious Material (CM)	**Polymer-modified CM and polymer concrete**
Strengths	• Compatible to substrate • Low cost • High availability • Easy placing and finishing • Aesthetic aspect • Resilient to high temperature	• Mechanical properties • Low shrinkage • Shorting curing period • Resilient to aggressive environment

2.6 Correlation between durability testing techniques

There are insufficient studies on the correlation between concrete conductance measurements (i.e., RCP and surface/bulk resistivity), permeability measurements, and mechanical properties of concrete materials. Ibrahim and Issa [20] have reported the relationship between water permeability and RCP tests that water penetration depth was inversely proportional to the cumulative electrical charge. In their research, no correlation function was given but for highly permeable concrete, the total electrical charge increased significantly in comparison to the water penetration depth. Wongpa et al. [43] investigated the relationship between water permeability and compressive strength, according to which higher the permeability of cementitious materials, lower the compressive strength. Their findings agreed with those from the researcher who used conventional concrete

[44]. Snehal and Shekhar [45], Lübeck et al. [46], and Ramezanianpour et al. [47] reported a linear relationship between compressive strength and the surface resistivity of mixes that had similar ingredients. However, if all the data points from different mixes are plotted in one graph, the linear relationship can not be established [46], [47]. In terms of the relationship between test methods for evaluating concrete conductance, RCP and resistivity test results were found to be strongly correlated both theoretically and experimentally [14], [47]. The total electrical charge of concrete obtained from RCP tests can be expressed as a function of concrete resistivity, as demonstrated in Eq. 7 and Eq. 8 [34], [48]. Also, it was found that a linear relationship exists between surface and bulk electrical resistivity methods [48]. Some of the empirical relations established by other researchers are summarized in Table 3.

$$Q = I_{rcp} \cdot t = \frac{V_{rcp}}{\frac{L}{A} \cdot \rho} \cdot t = \frac{V_{rcp} \cdot A \cdot t}{L_{rcp}} \cdot \frac{1}{\rho_{bulk}} \tag{7}$$

$$\frac{\rho_{surf}}{\rho_{bulk}} = m \tag{8}$$

Where,

I and V are the electrical current and voltage respectively; t indicates the time duration of RCP test; ρ indicates concrete resistivity; A represents the cross-sectional area and L indicates concrete specimen length; Q is the cumulative electrical charge in coulombs; m is the ratio of surface and bulk resistivity which ranges from 1.9 to 2.63. The subscripts, such as rcp, bulk, and surf, represent the results from RCP, bulk, and surface resistivity tests respectively.

Table 3 Empirical relationship between test methods

Material	Test method	Relation	R^2	Ref.
ASTM Type I cement & silica fume & granulated blast furnace slag	RCP (x variable) & water permeability (y variable)	Parabolic (downward)	0.86	**[20]**
Rice husk – bark ash & fly ash	Compressive strength (x variable) & water permeability (y variable)	$y = (0.1814)x^{-6.265}$	-	**[43]**
Ordinary Portland cement & rice husk ash & fly ash & steel fibers	Compressive strength & bulk electrical resistivity	Linear (only for similar mixes)	-	**[45]**
White Portland cement & blast-furnace slag	Compressive strength & surface electrical resistivity	Linear (only for similar mixes)	0.94-0.99	**[46]**
ASTM type I Portland cement	Compressive strength (x variable) & surface electrical resistivity (y variable)	$y = 0.2788x + 2.561$	0.87	**[47]**
ASTM type I Portland cement & metakaolin	Compressive strength (x variable) & surface electrical resistivity (y variable)	$y = 0.2567x + 0.0982$	0.77	**[47]**
ASTM type I Portland cement & silica fume & rice husk ash & metakaolin	Compressive strength (x variable) & surface electrical resistivity (y variable)	$y = 0.0196x^2 - 1.0519x + 25.776$	0.41	**[47]**

Chapter 3 Experimental investigation

3.1 Material and sample preparation

Three types of commercially available cement-based repair materials are used and termed as Mix F, M, and P in this project. Concrete patch materials can be roughly classified into three categories including cementitious concrete, polymer-modified concrete, and polymer concrete depending on the ratio of cement to polymer constituents in the mix design. Table 4 lists some key characteristics of the three repair materials specified by the manufacturers. Further details for each commercial mix as provided by the suppliers are in Appendix A. Because of the fast-setting characteristics of repair concrete, samples were prepared consecutively in small batches 4 times with the same w/c as per manufacturers' specifications.

Table 4 Material information provided by manufacturers

Mix	F	M	P
Category	Cementitious concrete	Cementitious concrete mortar	Fiber-reinforced (i.e., Polymer-modified) concrete mortar
f_c' * at 28 days of water curing (MPa)	50	62	50.3
working time (min)	30	75	6

*f_c' indicates the compressive strength

The concrete repair materials are mixed as per the manufacturer specifications. For Mix F, 2.45L of water was added per 25kg of material. Raw material was added to the mixing container and clean water was added to it after. The mixture was mixed for approximately 3 minutes using the paddle mixer attached to a 0.5-inch drill. The material was placed within 30 minutes of mixing. For Mix P, same preparation procedure was performed except the mixing ratio was 3.79L of water per 22.7kg of material and a much shorter working time at 5 to 6 minutes. Mix M has a mixing ratio of 2.15L water per 25kg and working time of 45 minutes maximum.

For different test methods, molds with different dimensions were used to satisfy our needs. Table 5 summarizes the information about specimen dimensions, and the standard they followed.

Additionally, the placement and consolidation process of concrete mixtures conform to the ASTM C 192 [49].

Table 5 Specimen dimensions and the standard information

Test method	Specimen dimension	Standard
Compression	4'' dia. x 8'' (cylinder)	ASTM C39
Surface/Bulk resistivity	4'' dia. x 8'' (cylinder)	AASHTO TP95/ASTMC1760
RCP	4'' dia. x 2'' (cylinder)	ASTM C1202
Water penetration	6'' dia. x 6'' (cylinder)	DIN 1048
Flexural strength/toughness	6'' x 6'' x 21'' (prism reinforced with 10M x 19'' rebar)	ASTM C293/ASTM C1609
Half-cell potential	6'' x 6'' x 21'' (prism reinforced with 10M x 19'' rebar)	ASTM C876

In order to determine the stress-strain behavior of the samples, strain gauges were also applied on 6'' x 6'' x 21'' prism specimens both on the rebar and on concrete surface, as shown in Fig. 4.

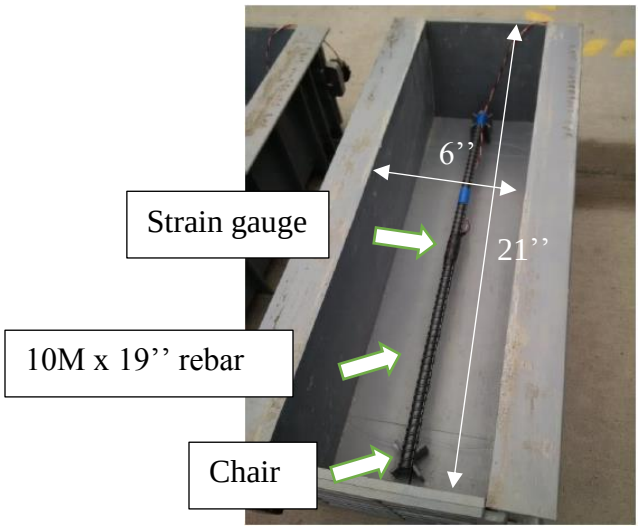

Figure 4 Specimen molds with chairs and rebar setup

Strain gauges were attached to the mid-section, underside of the reinforcement bar with 10 mm in diameter. The rebar is made from blackened steel which has better corrosion resistance compared to uncoated iron alloys. Since the specimens were submerged in an aggressive environment for long duration, special care was required when installing the strain gauges. The surface of the rebar was degreased and the ribs are grinded smooth using a grinder wheel for 3 inches in length at the center. The grinded surface was wet sanded using 220-grit paper. A gauze sponge was used to clean and dry the surface before adhesive application. M-Bond AE-10 from VPG Micro-Measurements was used to attach the CEA-06-125UW-120 strain gauges onto the rebar. After the strain gauge was fixed in position, another layer of M-Bond AE-10 was coated on top and FA-2 foil was used to cover the coating for additional mechanical protection. For additional protection against aggressive species under immersion, M-Coat B was applied to seal all the edges of the foil and finally a layer of M-Coat JA was applied for environmental protection of strain gauge installations.

For RCP testing, it normally takes two days for the sample preparation procedure. Hence, after 26 days of curing, specimens were moved out of the water tank and sliced using a wet tile saw into the size of 100mm diameter and 50mm long. It should be noted that the top surface of the cylinder, which serves as the datum plane, was first ground so as to attain the desired flatness. Each surface being cut was further polished on a grinding machine for two minutes for a better surface finish. The cutting and grinding processes are shown in Fig. 5 In addition, the side surfaces around the circumference of concrete disks were coated with epoxy resin to force chloride ion penetration to be one-dimensional and to prevent any lateral flow.

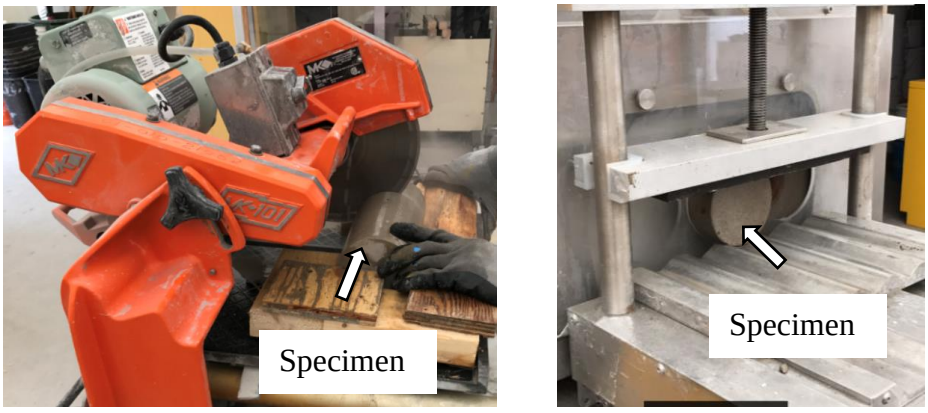

(a) (b)

Figure 5 Specimen cutting and grinding process (a) Specimen cutting on a wet-tile saw(b) Specimen end surface grinding

Since concrete is a nonconductive material, water is used to saturate the specimens to increase the transportation of chloride ions. At 27 days of curing, a vacuum chamber was employed to extract the pore solution from the specimens. A vacuum pump, which can maintain a pressure of less than 6650Pa, was connected to the chamber and was running for 3 hours to fully evacuate the vacuum chamber. The distilled water was then injected into the vacuum chamber and submerged the samples while keeping the vacuum pump running for an extra hour. The specimens were left immersed in water for 18 ± 2 hours after which the specimens were ready to be tested. The water saturation setup is shown in Fig. 6. It should be noted that a desiccant bottle was mounted between the vacuum chamber and the pump in case the water goes into the pump.

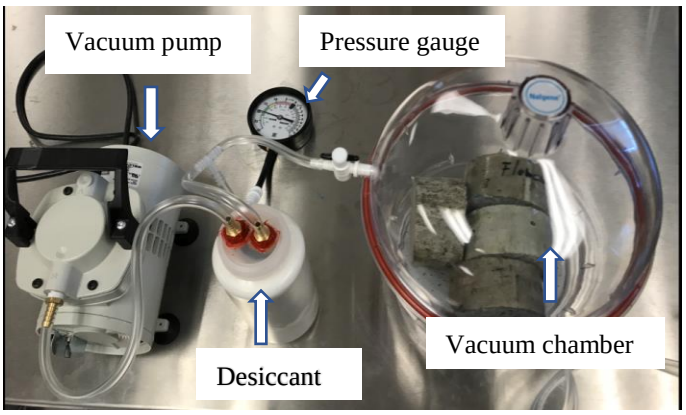

Figure 6 Water saturation setup

3.2 Curing and additional preparation

Concrete test specimens for compressive strength and bulk/surface electrical resistivity tests were demolded 24 hours after casting, and water cured in the curing chamber at 23 plus or minus two degrees Celsius until the testing day following ASTM C31 [50]. Compression test was performed on 1-, 3-, 7-, 28-, and 70-day specimens in accordance with ASTM C39 [51]. Accordingly, the surface resistivity test was performed every 14 days after 28 days of immersion and up to 70 days of curing ages. These specimens were then immersed in the sodium chloride solution with a concentration of 35 parts per thousand (ppt) for another 14 and 28 days to simulate conditions experienced by concrete repair in marine applications. Bulk electrical resistivity tests were conducted on 90-day samples cured in tap water at 23 plus or minus two degrees Celsius. It should be noted that half-cell potential was measured one year after sample casting and specimens were treated with chloride solution at ambient and elevated temperatures. The curing conditions of

specimens for flexural properties measurements (strength/strain/toughness), RCP, surface resistivity (SR), bulk resistivity (BR), water penetration (WP), compression, and half-cell potential (HC) test methods are summarized in Table 6.

Table 6 Curing conditions for all tests

Mixes	Test ages (in days)						
	RCP	SR	BR	WP	Comp	HC	Flexural properties
F	28	28; 42; 56; 70; 70(14); 70(28)	90	28	1; 3; 7; 28; 70; 70 (14)	365*	365*
M	28	28; 42; 56; 70; 70(14); 70(28)	90	28	1; 3; 7; 28; 70; 70(14)	–	365*
P	28	28; 42; 56; 70; 70(14); 70(28)	90	28	1; 3; 7; 28; 70; 70(14)	365*	365*

Notes:
1. All numbers under test ages indicate the days immersed in tap water at ambient temperature ($23 \pm 2°C$) unless otherwise stated.
2. The number in parenthesis indicate the additional days of chloride immersion in simulated seawater at $23 \pm 2°C$.
3. The asterisk means special treatment which includes a 70-day tap water (at $23 \pm 2°C$) immersion, a 28-day simulated seawater immersion ($23 \pm 2°C$), a 14-day simulated seawater immersion at $60°C$, and exposure to open space until it reaches one-year old

For flexural property testing, as curing time was over, strain gauge was attached to the midspan at the centerline of the bottom surface closer to the reinforcement. Firstly, a stiff-bristled brush was used to clean the concrete surface to remove loose soil. The M-prep conditioner A and the M-Prep Neutralizer 5A was applied with the gauge sponge after which the surface was rinsed with water. This step aims to clean any dust and other contaminants that remain on the surface. After this, the heat gun was utilized to dry the surface thoroughly and the epoxy resin was applied to fill the pores since concrete is a porous material. As epoxy resin hardened, the surface was roughened with the

320-grit abrasive paper in order to promote the bonding force later by enlarging the contact surface area. In the end, M-bond 200 adhesive and catalyst were used to adhere strain gauges to the concrete surface. The strain gauge installation process follows the standard provided by the strain gauge supplier Micro Measurements [52].

3.3 Specimen testing

3.3.1 Compressive strength

Compressive strength of cylindrical concrete specimens was measured as per ASTM C39 [51]. The top and bottom of the cylinders were ground using the Humboldt automatic cylinder grinder to ensure flat and smooth surface for evenly distributed stress. As the specimens were taken out from curing tank, the surface water was blotted off and then specimens were placed on the compression machine for testing. A total of two specimens of the same mix design were tested and averaged in this study. Our test was performed on a Forney compressive machine with an loading rate of 0.25MPa/s, and the setup is shown in Fig. 7.

Figure 7 Compression test on Forney machine

In addition, Eq. 9 was used for calculating compressive strength:

$$\mathrm{f} = \frac{P}{\pi r^2} \tag{9}$$

where f is compressive strength, P is the peak loading force, r represents the radius of the specimen.

3.3.2 Flexural strength/toughness/strain

Flexural strength was determined following ASTM C293 [53], standard test method for flexural strength of concrete using simply supported beam under the center-point loading. The test schematic is shown in Fig. 8. The flexural strength was calculated based on the maximum applied load indicated by the MTI Universal testing machine. Eq. 10 was used to calculate the flexural strength (modulus of rupture):

$$R = 3PL/2bd^2 \tag{10}$$

where, R is the modulus of rupture in MPa, P is the maximum center-point load in N, L indicated the specimen span in mm, b is the width of the specimen in mm, d is the depth of the specimen in mm.

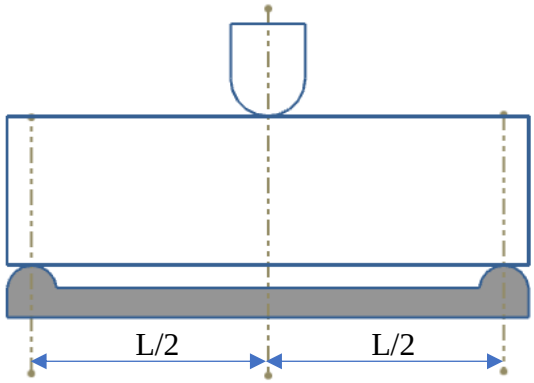

Figure 8 Flexural strength measurement under center-point loading

Apart from strength, flexural toughness is one of the most significant factors that engineers are interested in. It determines the energy absorption ability and the capability to withstand large deformations prior to failure. It is always preferable to have materials with high toughness applied in building structures because it takes long for the structures to experience a catastrophic failure in extreme conditions such as an earthquake, and thus provides more time for people to evacuate.

In this research, flexural toughness measurements were also performed on the MTI machine with only the addition of two digital dial gauges and a Japanese yoke, which surrounds the specimen and is clamped to the beam at the mid-depth directly over the supports. The two dial gauges were mounted on the yoke, one on each side so as to measure the average mid-span net deflection. In order to record the real-time data from the two dial gauges, two cameras were placed

correspondingly with one on each side as well. The Japanese yoke serves to counteract the extraneous effects of seating and twisting of the specimen on its supports or deformation of the support and loading system. The test setup is shown in Fig.9. The flexural toughness can be determined based on the area under the load versus deflection curve up to a net deflection of 1/150 of the span length.

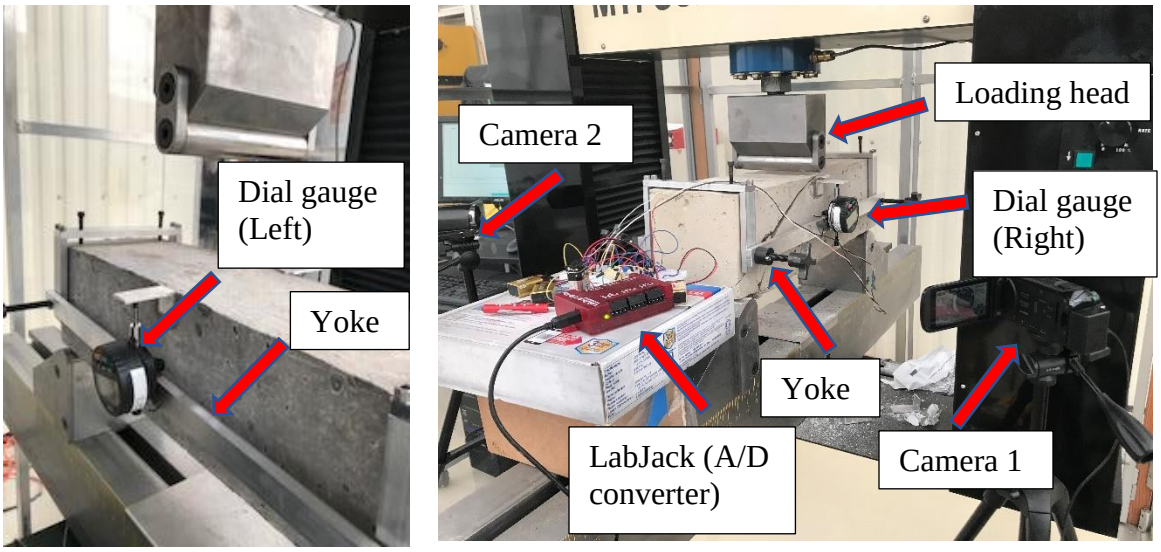

(a) (b)

Figure 9 Flexural property measurement setup (a) Left view (b) Right view

During the beam bending process, the strain of the specimen was monitored by the strain gauges. A two-channel Wheatstone bridge was developed and employed to convert the resistance input from strain gauges to the voltage output which was amplified through an instrumentation amplifier. The data acquisition is done by the Labjack U3-HV apparatus serving as an Analog/Digital converter which has an input range of plus or minus ten volts. The diagram of the strain acquisition setup is shown in Fig. 10 in which *Rx* represents the strain gauge. The software to monitor the test is LJLog which is a free software provided by LabJack Measurement & Automation.

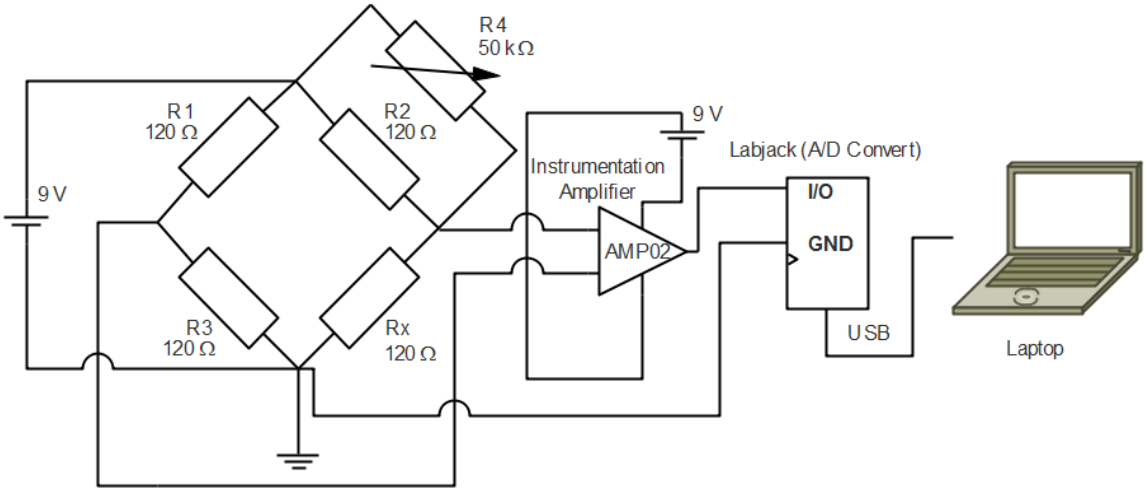

Figure 10 Schematic of strain acquisition

Based on the experimental setup, correlation between the strain gauge and the output voltage can be established, shown in Eq. 11 and Eq. 12.

$$\varepsilon_a = \frac{V_o\left(R_2 + R_x\right)^2}{V_s S G R_2 R_x} \tag{11}$$

$$G = \left(\frac{50k\Omega}{R_G}\right) + 1 \tag{12}$$

where, ε_a represents the strain value, V_o is the output voltage acquired by the laptop, R_1, R_2, and R_3 are bridge resistors having same resistance as strain gauge (120 Ω), R_x is the strain resistor (120 Ω), *S* represents the axial strain gauge factor (2.145), G is the amplifier gain, R_G is resistance (200 Ω) for gain control.

3.3.3 RCP test

On the testing day, specimens were transferred to the RCP testing cells. In our test, we used Giatec Perma2 RCP testing setup which consists of a data acquisition box (DAQ) and four testing cells, as shown in Fig. 11. One surface of the specimen was in contact with 3% NaCl solution while the other was exposed to 0.3 normal NaOH solution. A 60-volt DC potential was maintained across the samples for 6 hours during which the electrical current passed and the temperature change were recorded. The total electrical charge in Coulombs during the 6-hour period was regarded as an indication of the resistance of the samples to chloride ion penetration as per ASTM C1202 [32].

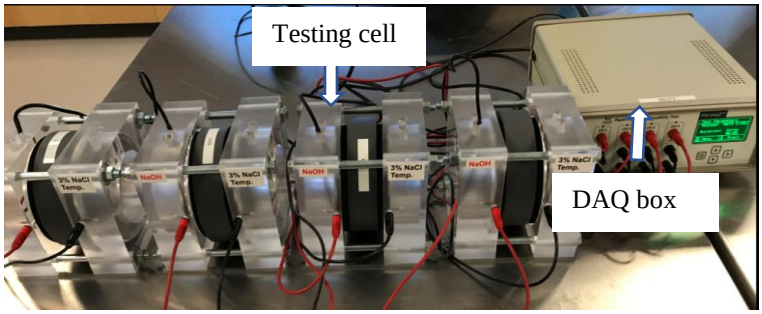

Figure 11 RCP test setup

It should be noted that some verifications were made prior to conducting RCP test. These measures include accuracy validation of the DAQ system, leakage inspection of the test cells, and temperature controls. Giatec Perma2^{TM} provides with a verification kit for verifying the accuracy of the DAQ device and control the quality of test results. By connecting DAQ correctly with the verification kit, the results showing "pass" or "fail" were displayed on the LCD screen, as shown in Fig. 12.

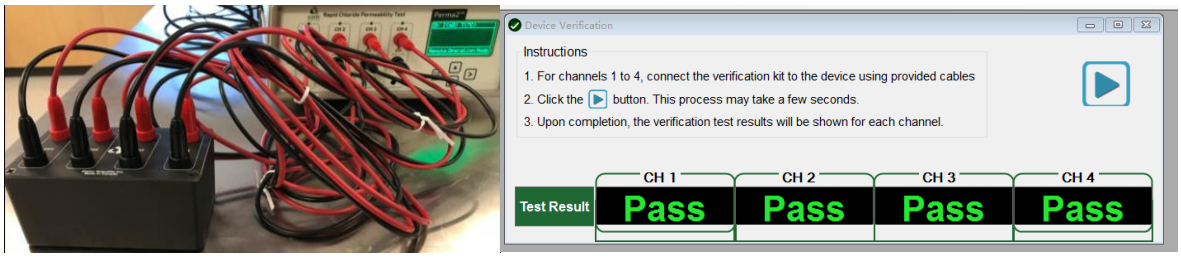

Figure 12 DAQ system verification

As all the channels have passed the verification test, leakage inspection should be performed to ensure a tight seal between all components of the apparatus. This test was conducted by observing the consistency of the solution level within 10 minutes or any dripping below. Lastly, environment temperature for conducting the test was tightly controlled ranging from 20℃ to 25℃. Additionally, the solution temperature during the test was also be strictly monitored and it cannot exceed 90℃ otherwise the test should be terminated. After all the verifications, the test was started by turning on the DAQ machine and left running for 6 hours.

3.3.4 Surface/Bulk resistivity test

In our study, Giatec Surf^{TM} apparatus was employed for resistivity measurement, as shown in Fig. 13(a). As can be seen, the sample holder has four sets of electrodes, placed at 90-degree array. Before the experiment, probe distance (denoted "a") was adjusted to be 1.5 inches (or 38 mm) and the electrical current frequency was set to 13 Hz in accordance with AASHTO TP95 [54]. Also, generous amount of conductive gel was applied to the tip of the electrodes in order to improve the electrical connectivity of the electrodes and the surface of the concrete. Once the test started, the apparatus ran two rounds so that eight measurements were taken and then averaged to obtain the resistivity around the test specimen.

In bulk resistivity measurement, the corresponding test setup is shown in Fig. 13(b). Specimens were taken from the curing tank just before the test started and blotted off the surface water in order to achieve the surface saturated dry condition (SSD). The concrete specimen was placed between two parallel metal plates which were connected to an alternate current source. Additionally, a wet sponge was sandwiched between the concrete specimen and the metal plate to maintain the electrical continuity during the test. The frequency of electrical current was set 1 kHz during the test due to the fact that high frequency can eliminate the polarization effect when measuring the resistance of concrete specimens.

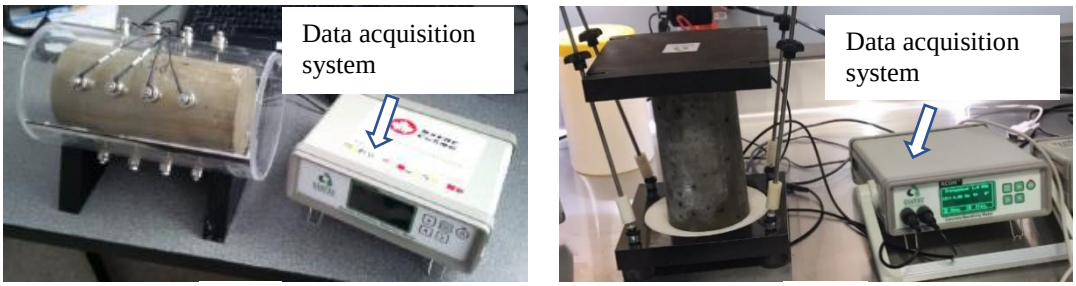

(a) (b)

Figure 13 Resistivity test (a) Giatec Surf ^{TM} test setup (b) Giatec RCON2^{TM} test setup

3.3.5 Water penetration test

The water penetration test was performed on six specimens at a time using the apparatus as shown in Fig. 14(a). A water pressure of 5 bar (0.5 N/mm^2) was imposed on the bottom surface of the specimen for three days as per DIN 1048 standard [12]. This pressure was generated by means of

the pressurized nitrogen gas applied to the burette, and was monitored and controlled through the pressure gauge and a regulator. In case of water leakage, a rubber gasket with 100 mm diameter was placed under the specimen and some silicone grease was applied to the gasket surface to further increase water tightness. The pressure was maintained for 72 hours, after which specimens were split into two halves by means of the direct tensile test. As shown in Fig. 14(b), the cylindrical specimen is placed on its side and loaded with diametral compression so as to induce transverse tension. The water penetration profile was then marked and used to calculate the coefficient of permeability which indicates the resistance to water penetration of concrete samples.

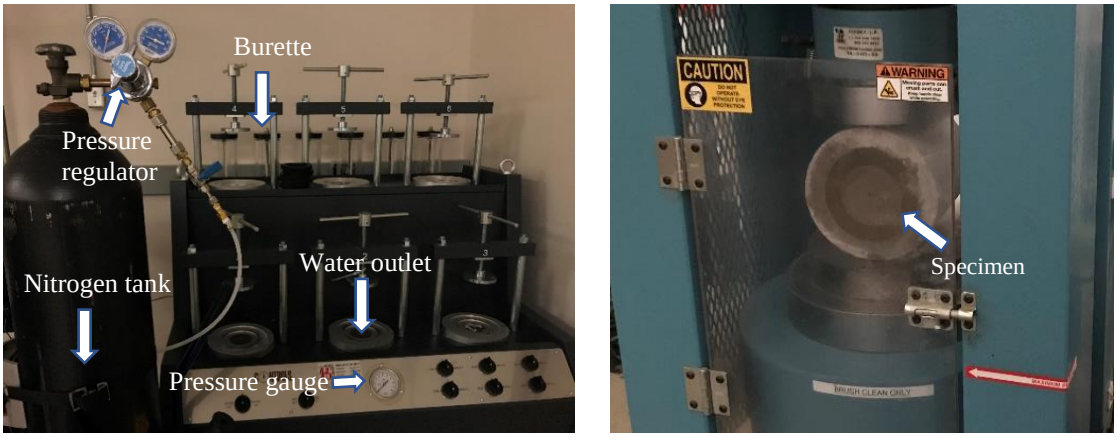

(a) (b)

Figure 14 Water penetration test (a) permeability test apparatus located in Facility for Innovative Materials & Infrastructure Monitoring (FIMIM) (b) Forney compressive test machine

The coefficient of permeability can be calculated using the water penetration results. According to modified Darcy's Law **[55]**, the depth of penetration can be expressed as:

$$\frac{\mathrm{dx}}{\mathrm{dt}} = k_w \frac{h}{x} \tag{13}$$

where x represents the depth of penetration (m), t indicates the experiment time (s), h is the water head (m), k_w is the coefficient of permeability. By integrating the equation and plugging in the initial condition, that is,

$$x\left(t=0\right)=0 \tag{14}$$

the k_w can be obtained as shown below:

$$k_w = \frac{x_w^2}{2ht} \tag{15}$$

Where, $\boldsymbol{x_w}$ represents the maximum depth of water penetration. After splitting the specimen, it can be observed that the penetration depth is not uniform across the sample's cross section (y-axis), as shown in Fig. 15. Also, it should be noted that the use of Darcy's law is based on several assumptions:

i. Concrete material is homogeneous;
ii. The velocity of water penetration does not change with time

Because the way specimen is split is random according to DIN 1048 **[12]**, it may result in a high standard deviation due to the heterogeneity of the concrete. In addition, because it takes some time for water flow to reach steady state condition, DIN 1048 recommends measuring the maximum depth of water penetration and divide that by the time to calculate average penetration velocity.

An example of Mix P after water penetration test is shown in Fig. 15, where W_{max} represents the maximum width of water penetration. *A* represents the wetted area.

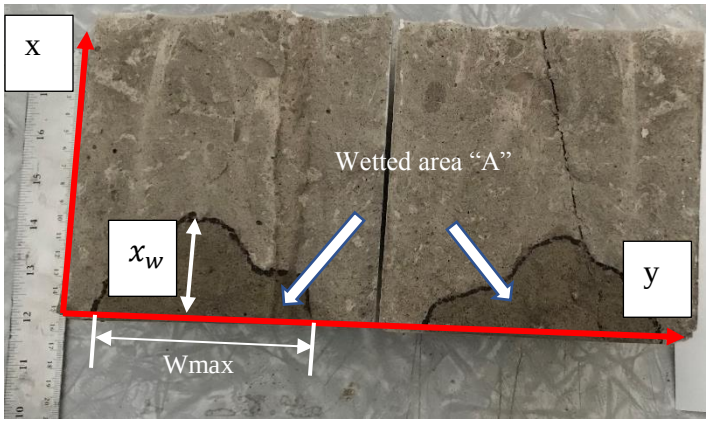

Figure 15 Profile of depth of water penetration (mix P)

3.3.6 Half-cell potential test

The half-cell potential test was conducted on reinforced concrete prisms with a dimension of 6 inches by 6 inches by 21 inches. After the specimens were demolded, they were immersed in tap water for 70 days, then in the simulated sea water with 35ppt salinity at ambient temperature for

28 days, and simulated sea water with 35ppt salinity at 60 degrees Celsius for 14 days. Additionally, these samples were left in an open space in BC Victoria for around one year before the test. Fig. 16. shows the schematic of the half-cell potential measurement setup. The copper/copper sulphate probe was used as the reference electrode and placed at the bottom of the specimens with a cover thickness of 0.5 inch and one inch. The measurements were taken on the bottom surface in a two by four grid for a total of 8 test points, following the ASTM C876 [56].

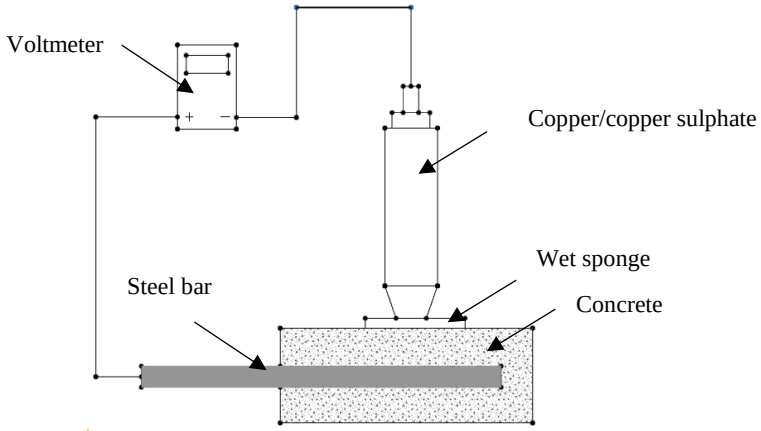

Figure 16 Schematic of half-cell potential test

Chapter 4 Results and Discussion

4.1 Compressive strength

Compressive strength results of specimens with 1-, 3-, 7-, 28-, and 70-day curing in water were obtained as well as the results of specimens immersed in simulated seawater for additional 14 days after 70-day normal curing. As shown in Fig. 17, each plotted point represents the average of two measurements, but unfortunately, the raw data was lost due to some reason and the standard deviation for each average point cannot be obtained. As illustrated in Fig. 17, all specimens gained strength during the initial curing stage. After 28 days of water curing, Mix F and Mix M matched or exceeded the compressive strength specified by the concrete manufacturers by 5 and 6 MPa respectively, as shown in Table 4. However, Mix P only reached about 40 MPa at 28 days which is lower than the manufacturer specification, 50.3MPa. Compared to the other two materials, Mix P has very short set time and a considerable amount of heat was generated during initial curing. It is possible that the excess heat generated and the following cooling process induced some initial microcracks within the concrete, thus, decreasing the strength of the specimens. Also, due to its fast-setting characteristics, six to ten seconds of compaction on the vibrating table may not be sufficient to remove large air bubbles entrapped in the sample, and thus affecting its strength performance. Therefore, longer compacting time or different curing regime may be required to achieve condensed specimens with lower porosity and higher strength. In addition, during specimen casting procedure, it can be observed that the workability of Mix F and M are better than Mix P, which is an important factor that needs to consider when using these products for repair work.

After 70 days of immersion, both Mix F and Mix M experienced a decrease in compressive strength but Mix P increased slightly. It is a common belief throughout the construction industry that after 28 days of curing, concrete can reach almost 100% of its strength. But depending on mix design or the hydration rate of the constituent, strength of concrete after 28 days of curing can still increase such as Mix P in our case. However, the measured concrete strength can be sensitive to environmental temperature and humidity as well as the degree of water saturation of concrete while tests were conducted. The strength reduction of Mix F and M may possibly result from the aforementioned factor, and thus more test results for these two mixes are required.

Additionally, as shown in Fig. 17, all three materials experienced a decrease in strength after 14 days of immersion in simulated seawater. Compared to steel-reinforced concrete, the effect of chloride ingress on the plain concrete specimen is relatively hard to predict. Shi et al. [57] reported that the strength of their mixes reacted differently (increase and decease) to continuous sodium chloride immersion. By using a scanning electron microscope (SEM) and conducting an Energy-dispersive X-ray spectroscopy (EDX) analysis, it was found that chloride ions can chemically react with the cement hydrates and form new products in the concrete matrix. In our case, the formed new product after the chloride solution immersion seemed to decrease the compressive strength of repair materials.

In general, the strength of concrete is defined by the strength of the cement paste and of the bonding between the paste and the aggregates. And it is widely believed that bond strength is largely dependent upon the Interfacial Transition Zone (ITZ) where the properties of the cement paste are different than the paste far away from the physical interface, in terms of morphology, composition, and density. ITZ usually has less crack resistance and thus can result in the weak aggregate-paste link so fracture occurs preferentially in this place [58]. Therefore, in order to better understand the strength reduction of our specimens due to chloride ingress, further research is required to investigate the chemical composition changes in both cement paste and ITZ before and after chloride immersion.

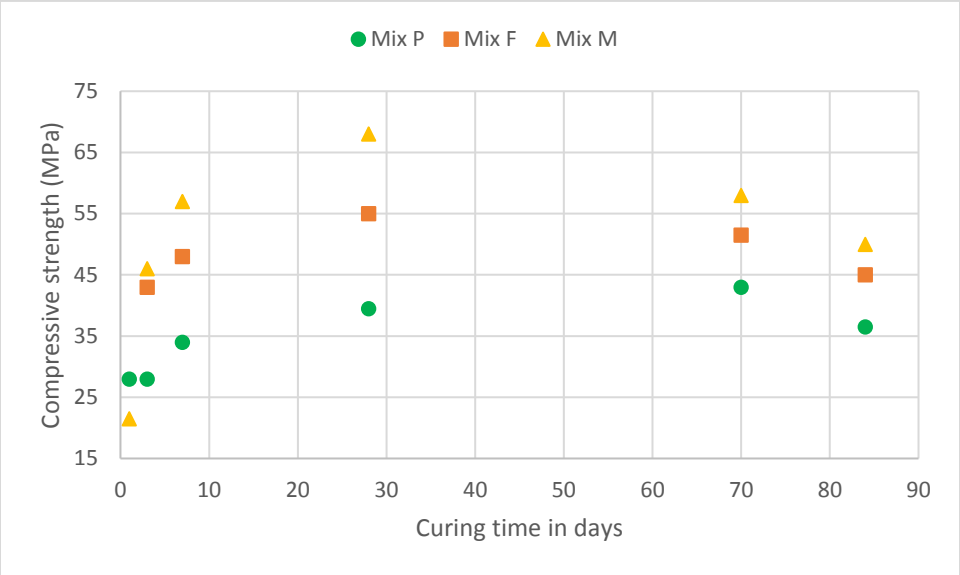

Figure 17 Results of compressive strength up to 84 days immersion

4.2 Electrical resistance

4.2.1 RCP

The resistance of three types of concrete to chloride ion penetration is evaluated by measuring the amount of electrical current passed through the samples in 6 hours. For Mix F, the electrical current recorded by the DAQ apparatus is shown in Fig. 18. The cumulative electrical charge, which geometrically indicates the enclosed area of the curve and coordinate axes, is obtained by integrating the current value with respect to time. Based on the calculations using the trapezoidal rule, specimen number three had the highest electrical charge followed by specimen number four, two and one. Accordingly, the temperature variations of these four specimens indicate that temperature increase is directly proportional to electrical charge, as shown in Fig. 19.

In addition, it can be obtained from Fig. 18 that specimen number two, three and four had consistent results, whereas the current value of specimen number one was only half the values of other specimens. This discrepancy was found to be as a result of the connection problem between the cable jack and the terminal, and thus the result of specimen number one was omitted while averaging electrical current of Mix F. This problem was solved by tightening the screws on the terminal before conducting the following tests. As shown in Fig. 18, the current values of all four specimens experienced a sudden drop at some certain points. The reason is that electrical current

is very sensitive to solution conductivity and temperature, so the gradually increased solution temperature and the constantly changed ionic concentration within pore solution can result in the fluctuation of the current values.

As summarized in Table 7, the average electrical charge of Mix F samples is 2669 coulombs, which according to ASTM standard C1202 [32], can be classified as having "Moderate" chloride ion penetrability at 28-day curing conditions.

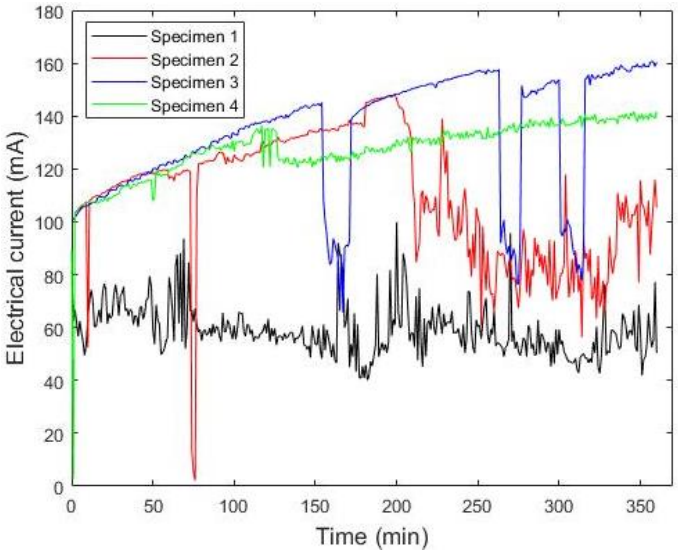

Figure 18 Current (mA) versus time (min) of Mix F

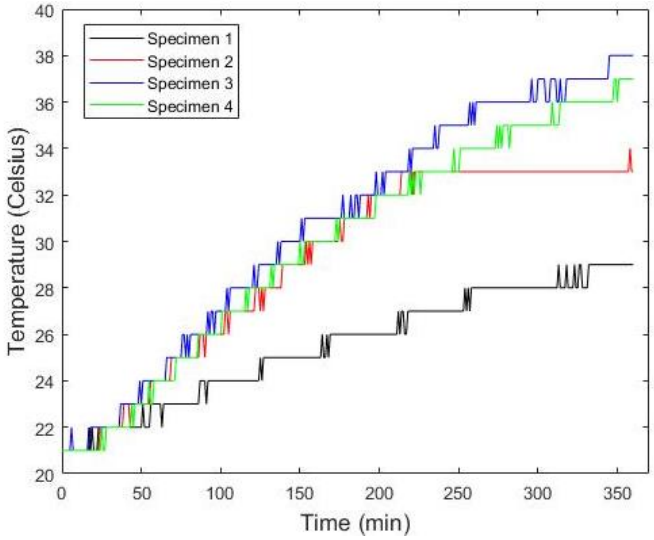

Figure 19 Temperature fluctuation (Celsius) of Mix F

Table 7 Rapid chloride permeability test results of three mixes

Material	Type F				Type M				Type P			
No.	I	II	III	IV	I	II	III	IV	I	II	III	IV
Charge (Coulomb)	1275	2373	2879	2755	1399	1379	1389	1419	749	903	762	773
Average (Coulomb)	2669				1396.5				796.8			
Standard deviation	9.88%				1.22%				8.98%			
Temp. Difference	17 ℃ Max.				9 ℃ Max.				2 ℃ Max.			

For Mix M, current vs. time curve is shown in Fig. 20. It can be observed that all four specimens displayed consistent current values over the six-hour period and these values were lower than those obtained from Mix F. As can be seen in Fig. 21, it is also found that the maximum temperature difference of Mix M samples over 6-hour period is 9 ℃ which is lower than Mix F's (17 ℃), and this indicates the temperature's correlation with electrical current that passed through the samples.

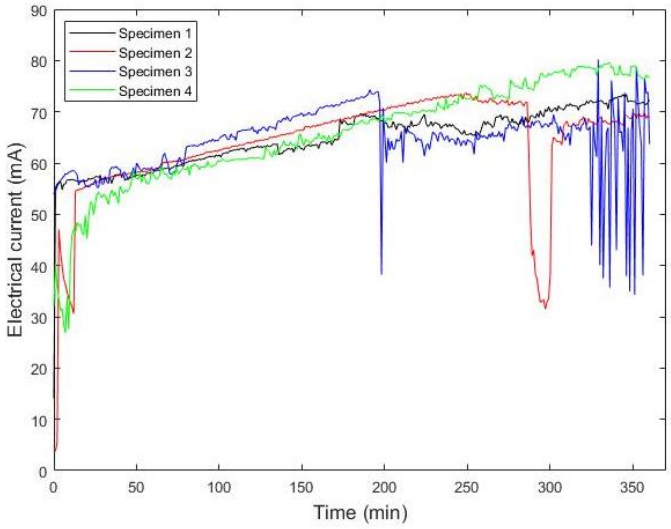

Figure 20 Current (mA) versus time (min) of Mix M

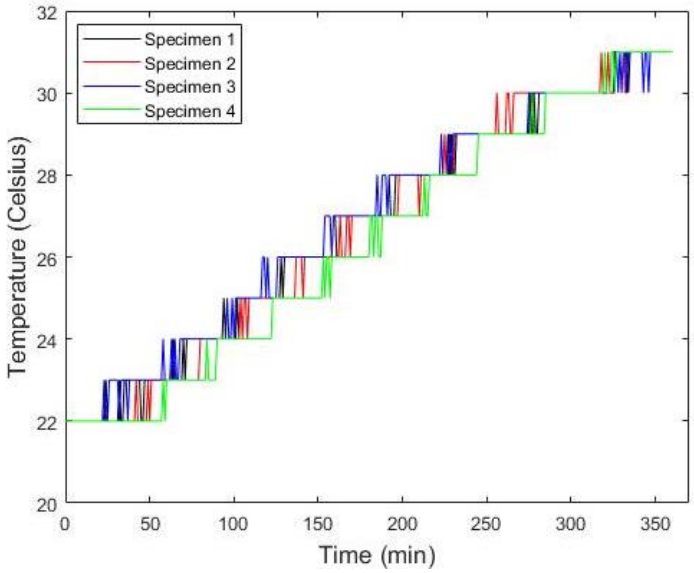

Figure 21 Temperature fluctuation (Celsius) of Mix M

As shown in Table 7, Mix M has an average electrical charge value of 1396.5 coulombs. In accordance with ASTM C1202 [32], it should have a “low” chloride ion penetrability. Fig. 22 and Fig. 23 show the current passed through Mix P and the corresponding temperature variations respectively. The cumulative electrical charge values are listed in Table 7. The cumulative electrical charge of Mix P samples is found to be 796.8 coulombs, which is regarded as a material with “very low” chloride ion penetrability.

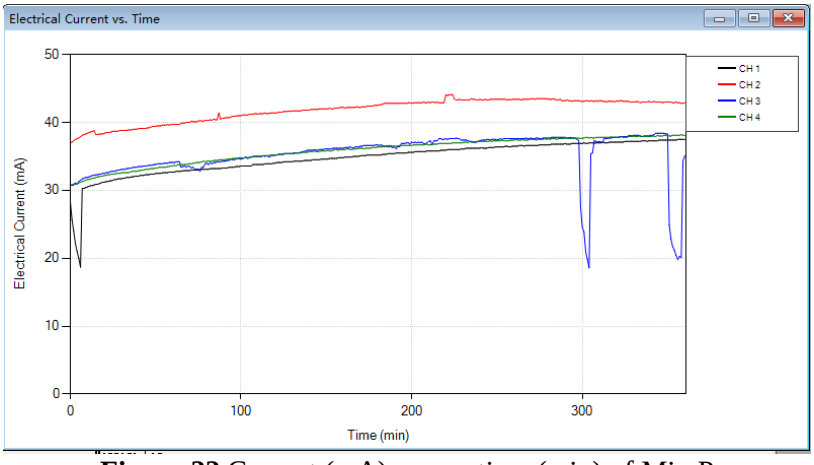

Figure 22 Current (mA) versus time (min) of Mix P

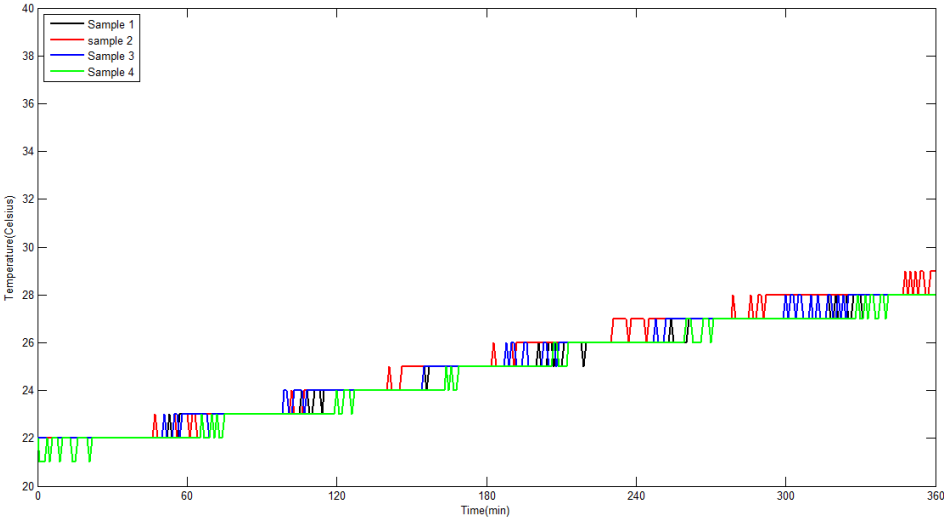

Figure 23 Temperature fluctuation (Celsius) of Mix P

4.2.2 Surface resistivity

The surface resistivity of all specimens gradually increases with curing ages, as shown in Fig 24. In general, Mix M has the highest resistivity which coincides with the compressive strength as Mix M being the material with the highest strength of the three. After the immersion in simulated seawater for 14 days, the results indicated that exposure to chloride has different effects on the three materials being tested. The surface resistivity of Mix M continues to increase after simulated seawater immersion and it seems unaffected by the introduction of chloride. On the other hand, Mix F experienced a dramatic drop from 95 kW-cm to about 40 kW-cm and Mix P decreased slightly in surface resistivity as well. This can result from the change in pore morphology and chemical composition of the pore solution after chloride ingress. Regarding concrete resistivity is dependent on the microstructures of the pores as well as the pore solution conductivity, further investigation is required to obtain the porosity information and chemical composition of the pore solution in order to better understand the mechanism behind the resistivity drop.

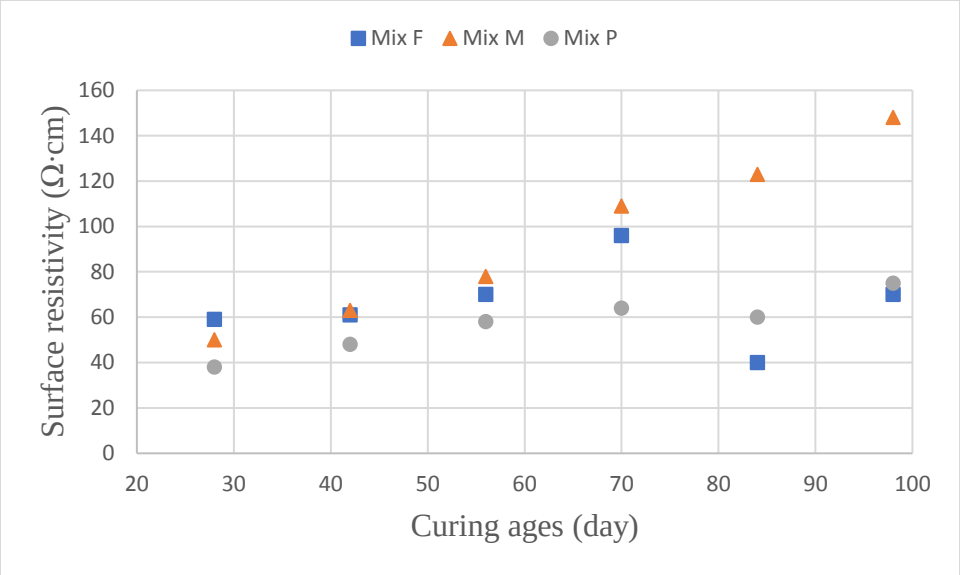

Figure 24 Surface resistivity of specimens using four points Wenner probe method

4.3 Water penetration

The water penetration results of Mix P concrete are presented in Fig. 15 as an example. It was found that the difference in water penetration depth between two halves was small, so the averaged maximum penetration depth x_a was calculated based on the average results from two halves. The coefficient of permeability was calculated using Eq. 15.

The test results are summarized in Table 8. It can be observed that Mix M has the lowest permeability coefficient followed by Type F and P, which shows some inconsistency with the findings of RCP tests. Based on the foregoing analysis in the literature review, the chloride ion penetrability should be proportional to the water permeability. There are several factors that could result in this inconsistency which includes different w/c ratio and measurement errors. Because of the fast-setting characteristics, repair material specimens cannot be cast in large quantities and thus results in slight w/c difference in different batches which are used for RCP and permeability measurements. Additionally, when measuring the penetration depth of samples using a tape measure, accurate depth values cannot be obtained due to the irregularity of the sample surface after compression.

Table 8 Water permeability results

Material	Type F			Type M			Type P		
	I	II	III	I	II	III	I	II	III
Maximum penetration depth $\times 10^{-3}$ m	15	13.5	13.5	7.0	11	6.5	47.5	75	32
Permeability Coefficient $k_w \times 10^{-8}$m/s	8.51	6.89	6.89	1.85	4.57	1.6	85.3	213	38.7
Average $k_w \times 10^{-8}$m/s		7.43			2.67			112	

4.4 Half-cell potential

The half-cell potential measurements of two different materials, Mix F and Mix P (Specimens of Mix M were lost), with a cover depth of 0.5 and one inch as indicated in parentheses, are summarized in Table 9. The data points are evaluated based on eight measurements across the bottom surface of the specimens closer to the rebar. The average measurement values were adopted here as per ASTM C 876 [56] because the variation between measurements is less than 150mV. As shown in Table 9, the results of Mix F (0.5), Mix F (1), and Mix P (0.5) are more positive than -200mV, which indicates there is a greater than 90% probability that no rebar corrosion occurs in the tested area. The half-cell potential of Mix P (1) is in the range of -200 mV to -350 mV, which indicates the corrosion activity of the reinforcing steel in measuring area is uncertain.

However, the half-cell potential measurements can only predict the probability of steel corrosion, while people are usually more curious about the link between steel corrosion and the failure of the structures. Probability risk assessment is a powerful tool, which can be employed to have a comprehensive and systematic assessment on the feasible detrimental outcome of steel corrosion [59]. The risk is the product of two quantities, i.e., the magnitude of the possible adverse consequence and the probability of the consequence which can be acquired from half-cell potential tests. The adverse consequences after steel corrosion can be obtained from the field application of repair materials, which requires further investigations in the future.

Table 9 Average half-cell potential measurements on prism specimens (after one year)

No.	1	2	3	4	5	6	7	8	Avg. (mV)
Mix F (0.5)	-89	-85	-84.3	-82	-82	-79	-76	-72	-81
Mix F (1)	-133	-123	-158	-206	-196	-154	-125	-136	-154
Mix P (0.5)	-235	-106	-138	-171	-185	-139	-145	-167	-161
Mix P (1)	-240	-243	-233	-251	-244	-231	-225	-234	-238

4.5 Correlation analysis

Concrete resistivity and conductivity are predominately controlled by two factors including microstructure properties (i.e., total porosity, tortuosity, pore size distribution, etc.), and the conductivity of pore solutions [47]. Both RCP and resistivity methods can characterize the mobility of moving ions, so it is reasonable to believe concrete with higher chloride penetrability will result in lower electrical resistivity. Assuming the resistivity of concrete specimens does not change over time, it can be concluded that RCP result is inversely proportional to the resistivity. However, in this study, no such relationship could be established between RCP and resistivity measurements. As shown in Fig. 25, the circular dots represent the obtained test value while the curve in blue color indicates the theoretical relationship between RCP and surface resistivity, which is derived from Eq. 7 and Eq. 8. It can be observed that among three mixes, samples have higher resistivity show higher RCP values. This phenomenon can result from the heating effect of the test method and from the binding effect of concrete materials which can significantly deviate the test results. Due to the high voltage (60 volts) imposed on the specimens, increment change in temperature will promote the mobility of all ions that carry the current, which in turn will raise the electrical current passed through the specimen [33]. Additionally, the binding effect can also affect the RCP value to a great extent. Since concrete is not inert to chlorides, chloride ions can bind with concrete physically or chemically. It was found by other researchers that chloride concentration, cement composition, temperature, supplementary cementing materials can all affect binding properties of the concrete [60], [61]. Therefore, concrete with high permeability and binding capability can show erroneously very low RCP values.

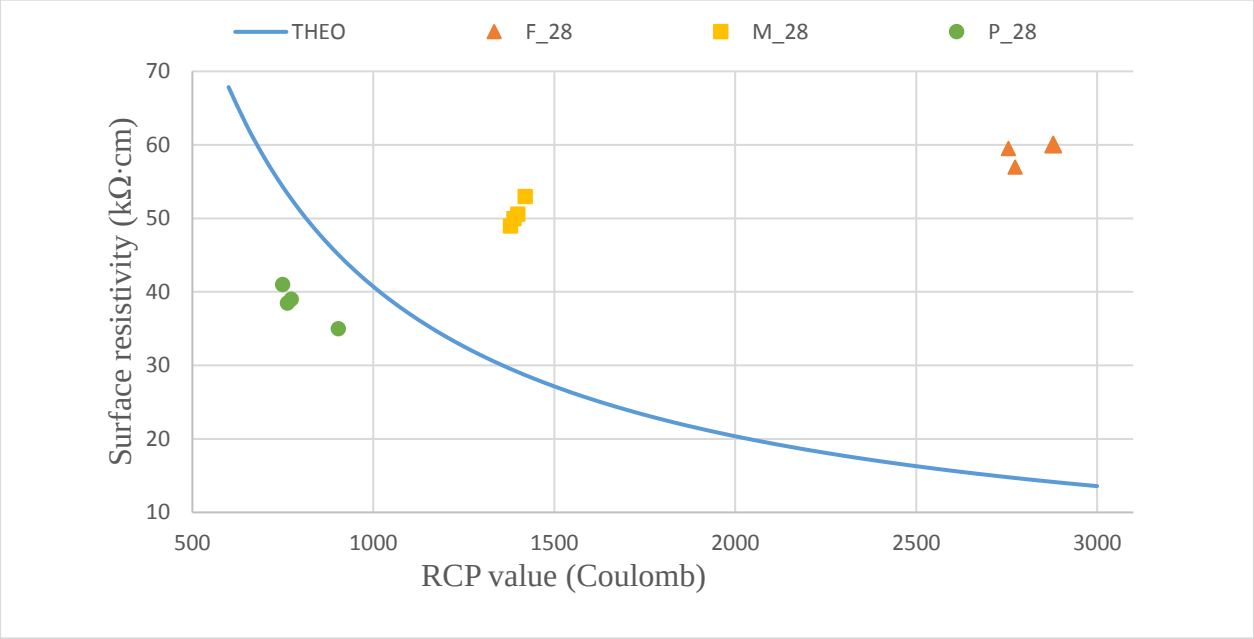

Figure 25 Correlation between RCP and surface resistivity test

Compression test is one of the most widely used tests to assess concrete's mechanical properties. As shown in Fig. 26, as the strength increases, the electrical resistivity increases correspondingly. However, for the same mix design at different curing ages such as P_28, P_70, and P_84, there is no relationship found between compressive strength and concrete resistivity. In addition, for all three mixes, the coefficient of determination of the regression line is only 0.3399 which indicates a weak correlation. The resistivity of concrete is dependent upon the pore microstructures and conductivity of the pore solution while compressive strength is largely affected by water/cement ratio (w/c), type and amount of cement, weather conditions amongst other factors. Therefore, pore microstructures, as well as the chemical composition of pore solution, have less effect on compressive strength compared to resistivity.

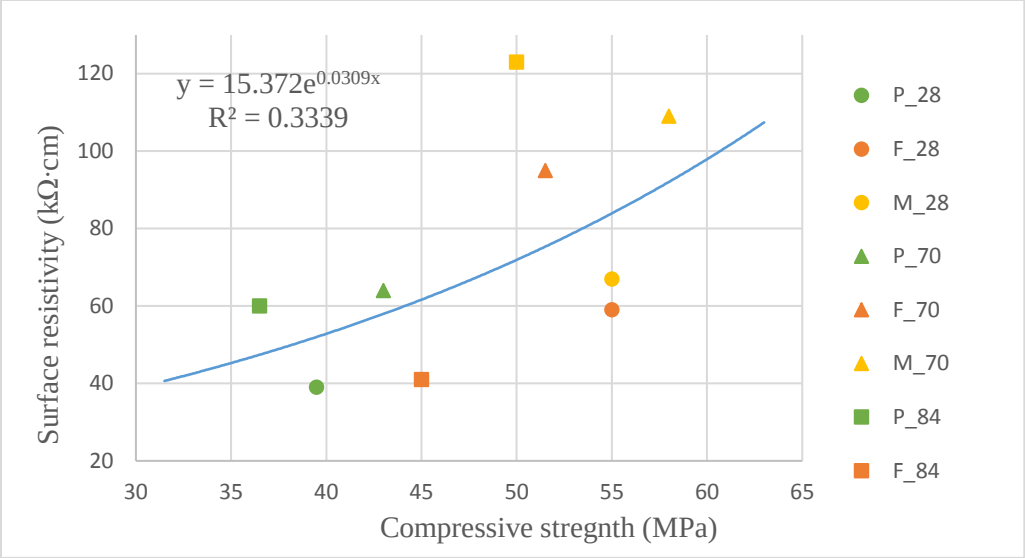

Figure 26 Correlation between RCP and surface resistivity test

The permeability, as well as the surface resistivity results, of the three mixes at 28-day curing ages, are plotted in Fig. 27. Test results are compared with the trendline from Ramezanianpour et al. [47] who tested 57 different mixtures made of ASTM C 150 type I Portland cement [62], rice husk ash, tuff, pumice, silica fume and metakaolin materials. As shown in Fig. 27, a power relationship can be found between our resistivity and water permeability results with a coefficient of determination value of 0.8573. At 28 days of curing, Mix M has the lowest water penetration depth followed by Mix F and Mix P. Meanwhile, surface resistivity value showed the same trend except that resistivity of Mix M and F are comparable. As seen in Fig. 27, concrete repair materials used in this study showed superior resistivity performance at the same water penetration depth in comparison to conventional concrete mixes.

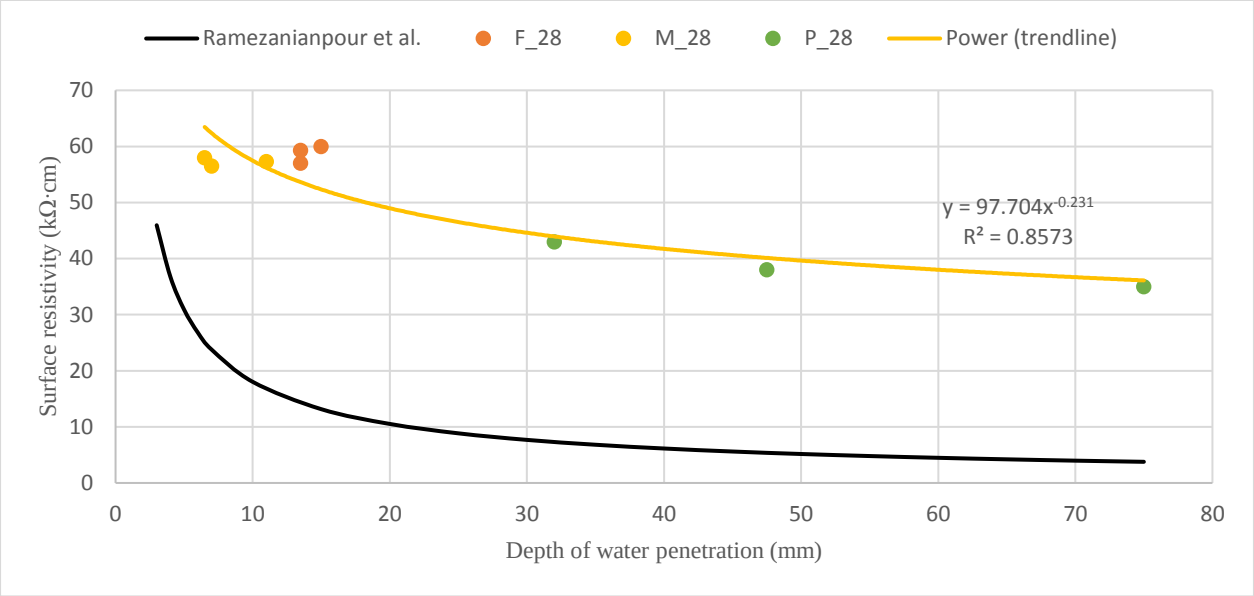

Figure 27 Correlation between permeability and concrete resistivity

As shown in Fig. 28, the compressive strength and surface resistivity values of three mixes are plotted against the curing ages. It can be observed that surface resistivity of all specimens gradually increases with the curing ages when they were immersed in the tap water (before 70 days). Similarly, all specimens gained strength during the early stage until Mix M and F experienced a slight drop after 28 days. However, after 28 days of curing, compressive strength and surface resistivity values showed opposite trend. As mentioned before, resistivity measurements are sensitive to pore solution which have less effect on compressive strength amongst other factors. After 70 days, specimens were placed in 35ppt simulated seawater and it can be found that chloride had a different effect on the three materials being tested. Both resistivity and compressive strength of mix F and P decreased, but the surface resistivity of Mix M seems unaffected by the introduction of chloride ions. Interestingly, the surface resistivity of all three mixes increased again after 28 days of immersion of sea water. This phenomenon can result from the conductance difference between chloride ions and other ions in the pore solution. For example, the conductance of hydroxyl ions is found to be approximately three times higher than chloride ions [47]. So, a high concentration of hydroxyl ions, which serves as providing an alkaline environment and protecting steel bar from corrosion, can produce misleading low resistivity values. Meanwhile, the conductivity of the pore solution is also dependent upon the binding effect of concrete materials.

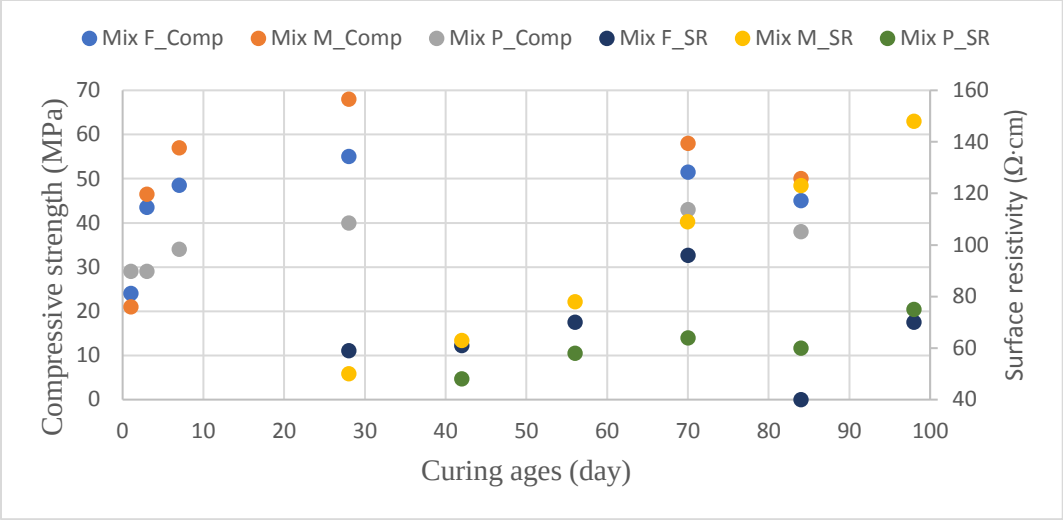

Figure 28 Results of compressive strength and electrical resistivity of concrete

As shown in Fig. 29, there is a strong linear correlation between surface and bulk electrical resistivity with a R^2 value of 0.9975. In the context of our study, the surface resistivity was found to be 2.08 times on average higher than bulk resistivity which supports the findings from other researchers, i.e., 1.86 (Spragg et al. [63]) and 1.9 (Gudimettla and Crawford [64], Azarsa and Gupta [65]).

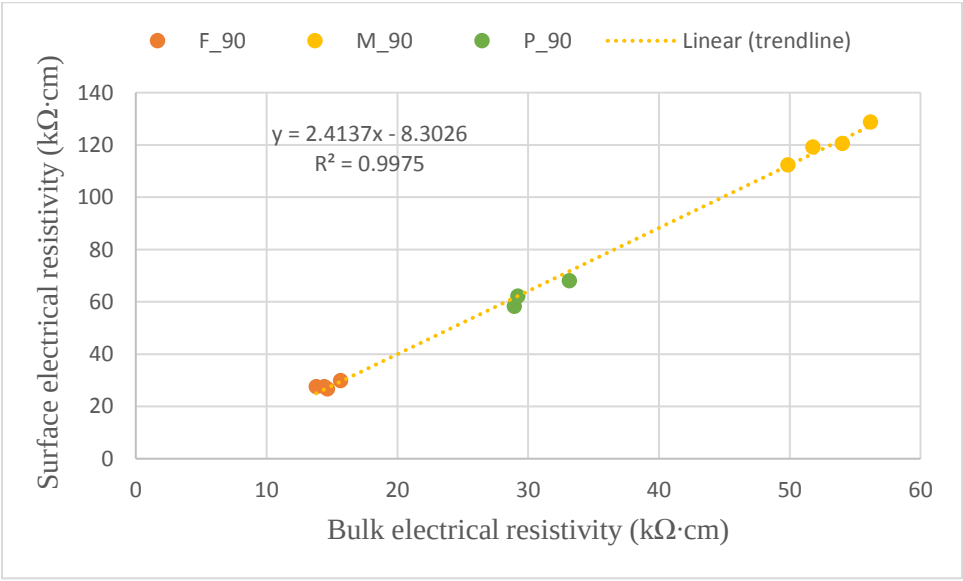

Figure 29 Correlation between surface and bulk resistivity

From previous results, no clear relationship was found between cover depth and half-cell potential values. In order to better compare various test methods, results of different tests obtained at 28 days of curing are plotted in Fig. 30. Results from different test methods are multiplied by different factors (either negative or positive) so as to fit into one graph, whereby the relative value between different tests and between different mixes using the same test method can be revealed. As shown in Fig. 30, materials with high compressive strength (Mix M and F) tend to have a high resistivity as well as low water penetration and vice versa. However, the RCP results do not conform to this trend, and materials with high electrical resistivity showed more chloride penetration in this study. In addition, half-cell potential results did not indicate much difference between materials, such as mix F and P, with different permeability and resistivity. This can result from the limited time span for testing because it may take several years for steel bars to corrode especially when using concrete with low water/cement ratios.

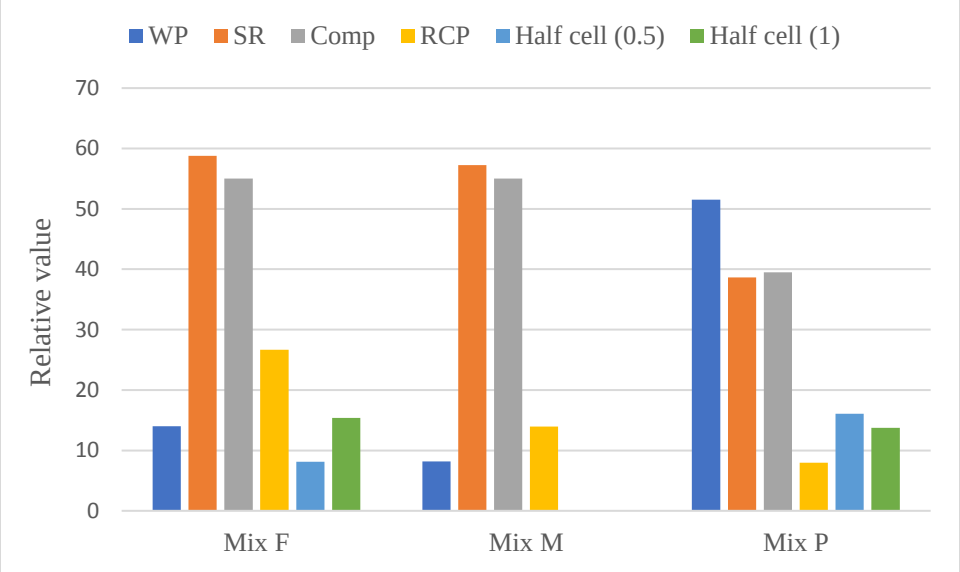

Figure 30 Data summary for various test methods

4.6 Flexural strength/toughness/strain

Flexural strength

Flexural strength of three types of specimens was acquired from MTI machine. Since all specimens were reinforced with steel bars, the flexural behavior is not only dependent on material properties

but the stiffness of rebars and their bonding strength. Also, Mix P has fiber addition which is expected to bridge the cracks and give higher flexural results. Fig. 31 shows the averaged modulus of rupture results corresponding to the peak load of three mixes, which consists of Mix F (7 specimens), Mix M (5 specimens), and Mix P (8 specimens). Also, the flexural strength of plain concrete, which is provided by material manufacturers, is also plotted. Further details for all the flexural responses of the specimens can be referred to Appendix B.

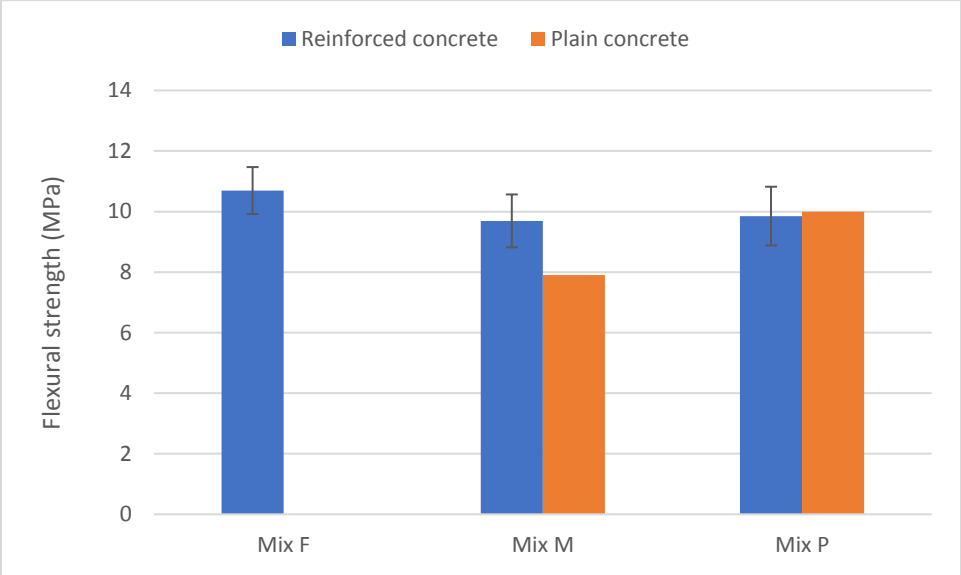

Figure 31 Flexural strength of average of three mixes

From Fig. 31, it can be observed that Mix F displayed the highest flexural strength followed by Mix M and P, which have comparable results. The concrete manufacturers provide with the material specifications that Mix M and P has a flexural strength of 7.9 MPa and 10 MPa respectively at 28 days of water curing. Compared with our results, addition of reinforcing steel greatly promotes the flexural performance of Mix M, yet flexural strength of Mix P seems unaffected. By further breaking the specimens of Mix P using a hammer, pores in millimeter scale inside can be observed as shown in Fig. 32, which did not exist in Mix F and M. In addition, during the flexural test, Mix M tends to have cracks, which initiated from the bottom support, propagated to its top surface, and caused failure due to the “pullout” of the rebar, as shown in Fig. 33. The aforementioned phenomenon can result from the material fast hardening and insufficient compaction that will lead to high porosity and weak concrete-reinforcement bonding.

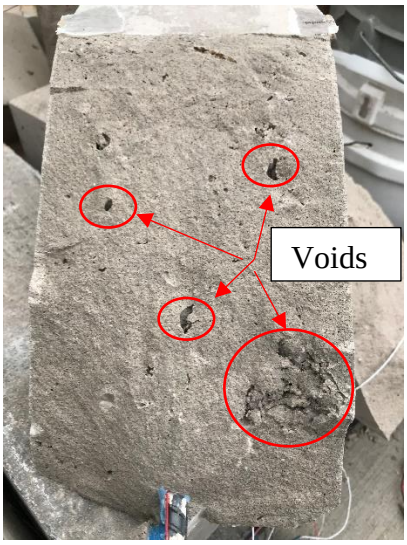

Figure 32 Beam cross section of Mix P

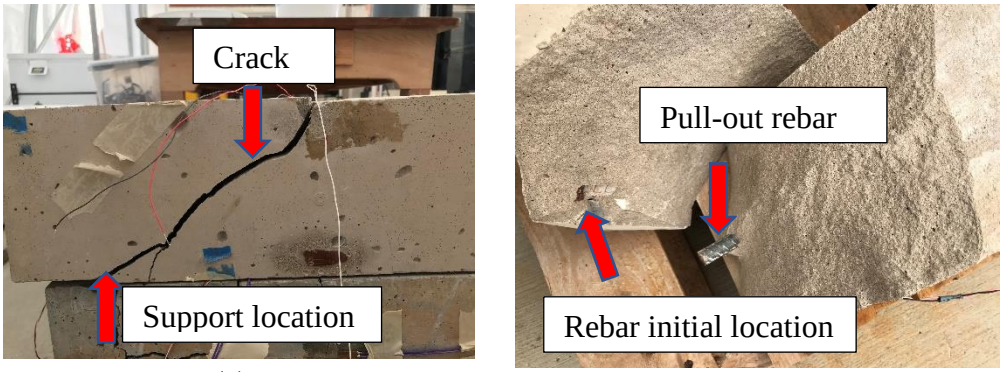

(a) (b)

Figure 33 Concrete prism failure due to rebar pullout (a) Crack pattern of Mix P after bending (b) rebar pullout

It should also be noted that some minor cracks were spotted on the Mix M specimens before the test started. However, the possibility of the cracks induced by steel corrosion can be ruled out because no appreciable rust can be observed on the steel surface. Therefore, the preformed cracks could be from the bulk expansion of material itself or due to some environmental factors such as alkali-aggregate attack and sulfate attack, which are beyond the scope of our discussion.

Flexural toughness

The flexural toughness can be determined by evaluating the area under the load versus deflection curve up to a net deflection of 1/150 of the span length. The load vs. deflection plot of Mix P is shown in Fig. 34 as an example. Point one and two in the graph show the first peak load and peak load respectively. Additionally, the first-peak strength, which is evaluated by plugging the first-peak load into Eq. 10, characterizes the flexural behavior of the fiber-reinforced concrete up to the onset of cracking.

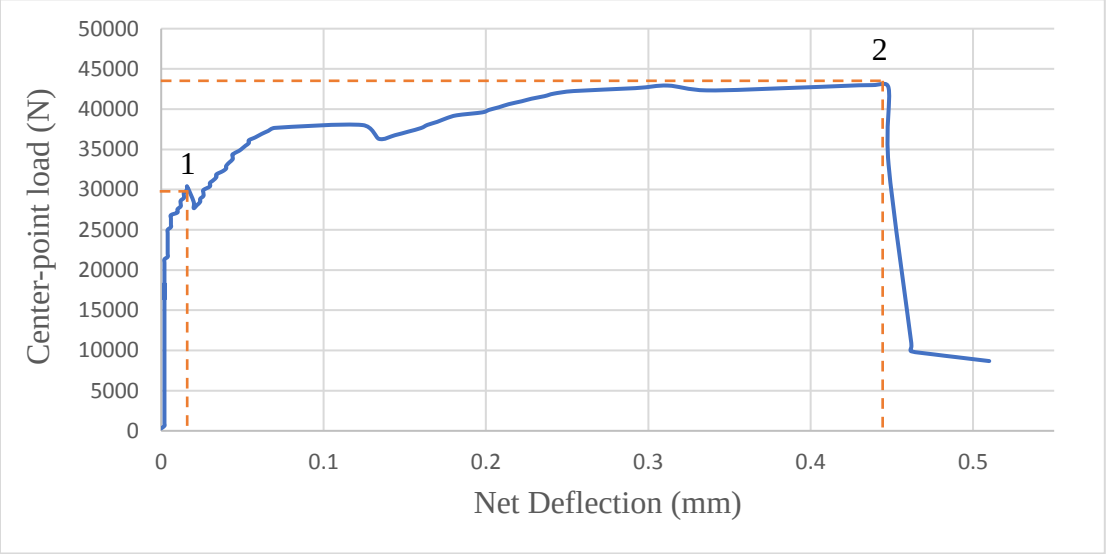

Figure 34 Load versus deflection of Mix P

The load was read directly from MTI machine while deflection was determined by the averaged values of two dial gauges mounted on each side of the beam. The flexural toughness results of three mixes are summarized in Fig. 35.

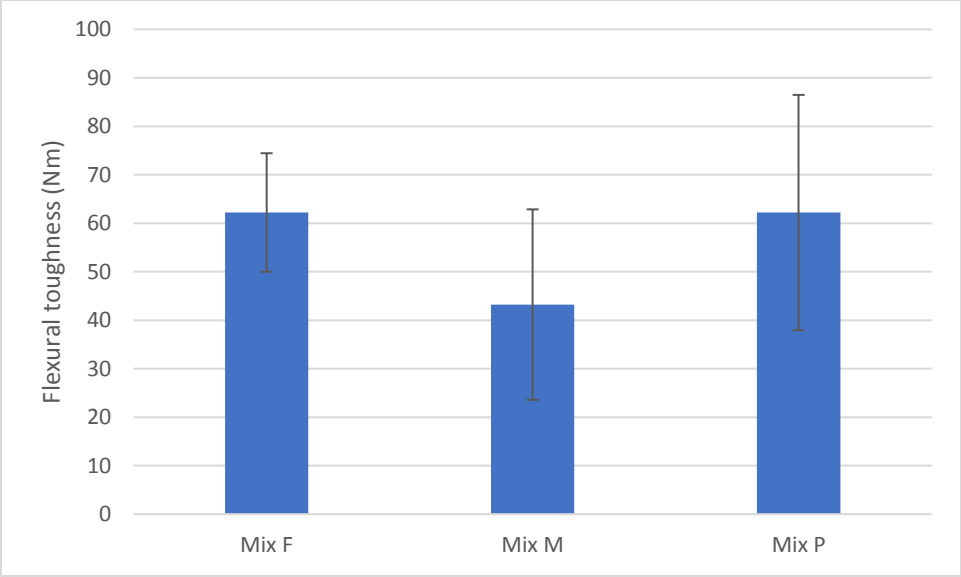

Figure 35 Flexural toughness on average of three mixes

From Fig. 35, it can be seen that Mix F and P had relatively the same flexural toughness of 62 Nm, while the flexural toughness of Mix M can only reach up to 43 Nm. Additionally, compared with conventional concrete which has a comparable compressive strength (ranging from 50 to 60 MPa at 28 days of curing [66]), our mixes with the addition of reinforcing bar show higher flexural toughness, that is, better the energy absorption capability. However, the standard deviation among specimens of each test is relatively high compared to flexural strength measurements, which may be because rebar bonding is coming into play. These testing errors were later found to originate from testing technique and setup. Unlike four-point bending, which applies force through two loading heads, center-point loading technique only use one and is prone to cause stress concentrations. Also, in theory, there is a pure bending moment zone in the middle third of the span for third-point loading condition, while for center-point loading unknow shear forces can run interference[58]. Additionally, the size effect of different testing techniques can also affect the scatter of test results. Since there is a relatively small portion of specimens, which is subjected to high stresses during the third point bending, the variation between different specimens could be large compared to the third-point method.

Flexural strain

Flexural strain results are obtained from the two strain gauges, one on the rebar and another one at the bottom of the beam, as sketched in Fig. 36. The strain on the rebar can be used to study the bonding strength between rebar and concrete. Because the maximum tensile strength of steel bars can reach up to hundreds of megapascal, while modulus of rupture of conventional concrete is usually below 10 MPa. So, the failure of steel reinforced concrete mostly results from the detachment of reinforcing bars but not from rebar failure, which was also observed in our tests. Assuming the rebars have the same elastic modulus, higher the strain on the rebar, higher the load carried by the rebar and thus better the bonding strength. Unfortunately, since strain gauge is super delicate and our specimens were kept in an open space for approximately a year, some of the strain gauges on the rebar were damaged and the wires connected to the strain gauges were pulled out during the transfer of specimens. Only a small number of strain gauges survived and their readings were recorded during the bending test. The results from strain gauges corresponding to the peak load of the specimens are summarized in Fig. 37.

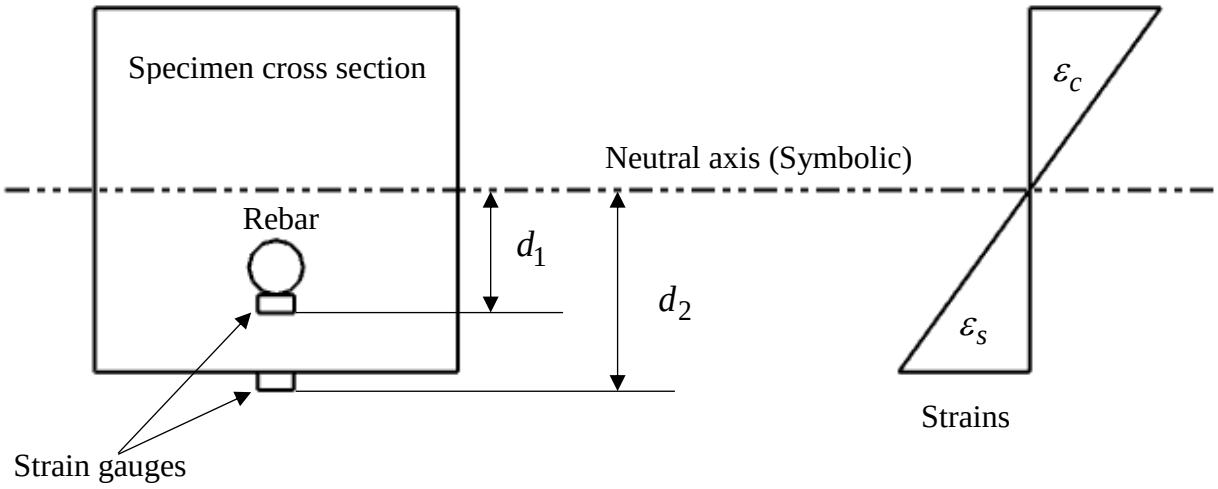

Figure 36 Strain gauge configuration and corresponding strains during bending

As seen in Fig. 37, at the peak load condition, Mix F has the best bonding capability with reinforcement because the average strain value on the rebar tops other two mixes, which agrees with the previous flexural strength results, shown in Fig. 31. Mix P did not show a good bonding

performance, but due to the addition of fibers in the mix design, flexural strength seems not largely affected by this factor.

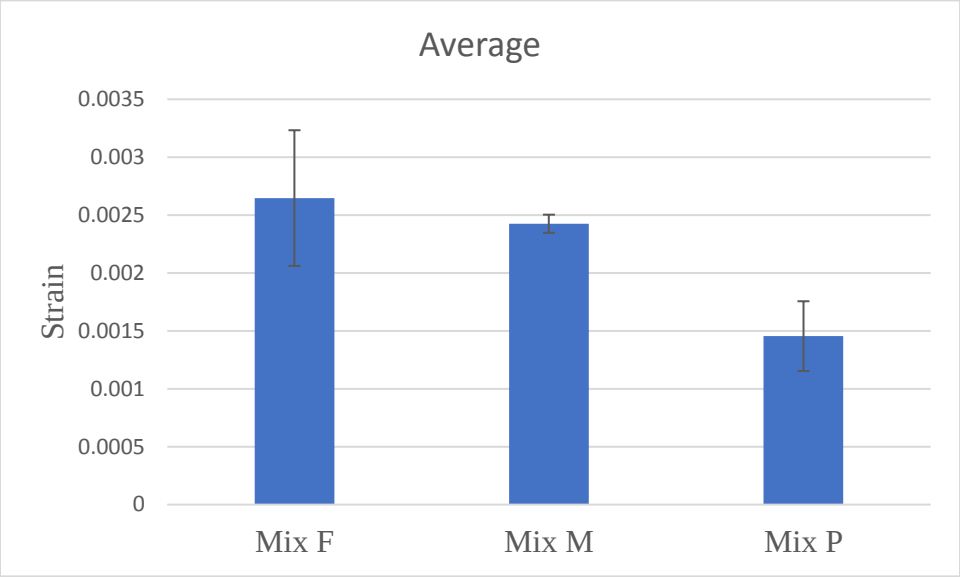

Figure 37 Maximum rebar strain of three mixes at the peak-load condition

In addition, strain gauge applied on rebar and beam bottom can be used to study the failure process of our specimens with reinforcement under tensile load. As shown in Fig. 36, it should be noted that the strain values above and below the neutral axes have opposite sign and corresponds to compression and tensile stress respectively. Also, all three mixes follow the same trend, and an example of Mix M was shown in Fig. 38. At the beginning of flexural testing, the strains are similar on the rebar and on the beam, with beam strain slightly higher than rebar strain due to the different distance to the neutral axis. At a certain stage, when cracks begin to form in the bottom of the beam, rebar strain experiences a dramatic increase because it starts to pick up the tension load which cannot be undertaken by cracked concrete. Then, rebar strain will gradually increase until it reaches its maximum value, after which it experienced a drop which indicates the onset of reinforcement detachment. But the rebar can still carry some load due to the friction force between the rebar and the concrete. After a couple of seconds when rebar is fully pullout from the concrete, the specimen experienced a destructive failure and both load and strain went to zero.

In addition, some analogy can be found between the failure process of our reinforced specimens and the pullout process of steel fibers from the concrete matrix. The basic pullout process consists

of two phases, adhesion phase and friction phase[67], [68]. At adhesion phase, adhesion shear bond exerts between fiber and matrix interface. Then, once the adhesion bond fails to resist the pullout load, the frictional shear bond will take effect, which allows the relative slip along the interface between fibers and matrices until the fibers are fully pulled out.

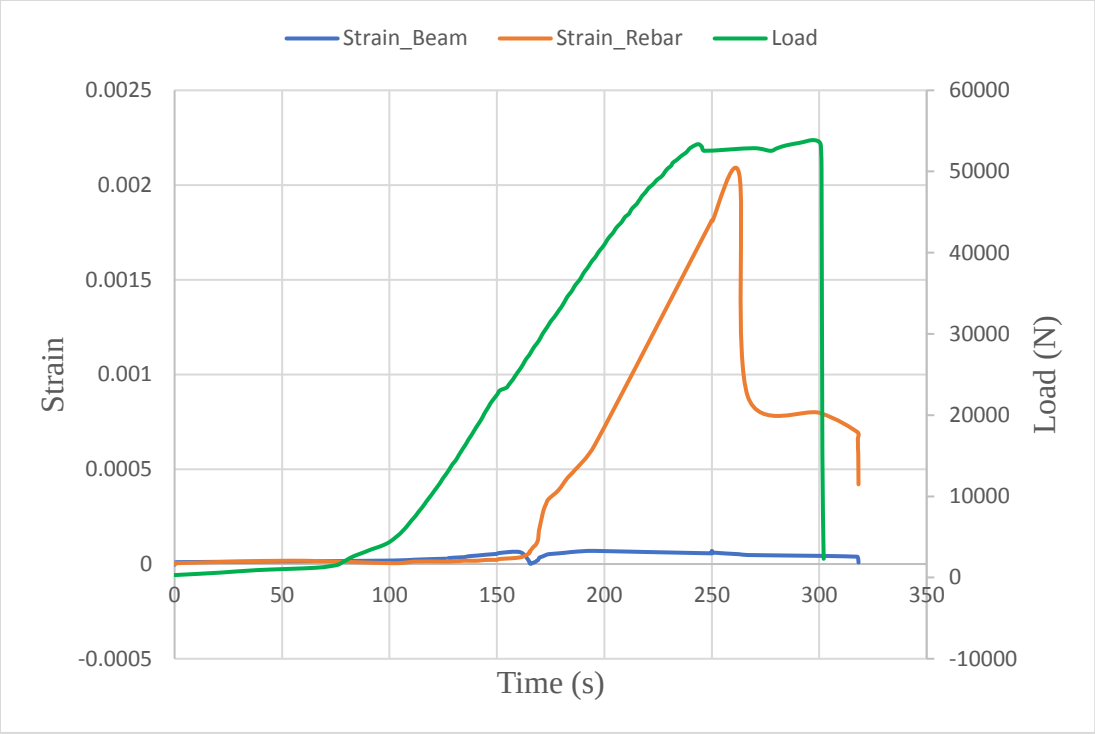

Figure 38 Strain gauge results and the load applied to Mix M

4.7 Chloride diffusion model with temperature adjustment

As mentioned before, penetration of aggressive ions can result from several mechanisms, such as permeation due to exterior pressure, diffusion due to chloride ion concentration, and capillary suction through the cracks due to capillary forces. Based on our water penetration test results, water permeability coefficient was calculated to quantify the chloride penetration via permeation process. Evaluating diffusion coefficient of repair materials requires the development of diffusion model for chloride ion transportation. However, due to the higher measured electrical charge caused by the heating effect, the previous model can overestimate the diffusion coefficient. So, in this section, a diffusion model with a temperature adjustment will be proposed based on our test results.

When the concrete is completely saturated with water, chloride ions penetrate concrete by a pure diffusion mechanism, in which concentration gradient is the driving force. The RCP results can be used to quantify chloride migration rate during chloride diffusion, and Nernst-Planck equation is normally used for describing this transport process[69]:

$$\mathrm{J}_i(x) = \frac{zF}{RT} D_i C_i \frac{\partial E}{\partial x} \tag{17}$$

where, $\mathrm{J}_i(x)$ is the unidirectional flux of chloride species ($\mathrm{mol}/(cm^2 \cdot s)$), z is the valency of chloride ions (z=1), F indicates the Faraday's number (96485.33 $\mathrm{C} \cdot mol^{-1}$), R is the gas constant (8.31 $\mathrm{J} \cdot mol^{-1} \cdot k^{-1}$), T represents the absolute temperature in Kelvin, D_i represents diffusion coefficient, C_i is the bulk concentration of the chloride ions ($0.512\,\mathrm{mol}/l$), E (60V) is the voltage applied to the concrete, x represents the longitudinal distance of the test specimen.

The unidirectional flux of chloride species $\mathrm{J}_i(x)$ can be correlated with the cumulative electrical charge during RCP test, and can be calculated using the equation below:

$$\mathrm{J}_i(x) = \frac{Q}{zAFt} \tag{18}$$

Where, A is the cross-sectional area of specimen, t indicates the time for RCP testing, Q is the cumulative electrical charge of RCP test.

In addition, for the sake of diminishing heating effect, some researchers proposed the correction function based on their test results [20], [33]. However, none of them was using repair materials and it is found that test results from our study do not follow their prediction equations. So, a new model is required, which can quantify the extra electrical charge during RCP test due to the temperature increase.

According to the first law of thermodynamics [70], internal energy (ΔE) of a closed system is equal to the amount of heat (q) supplied to the system, minus the work (W) done by the system on its

surroundings, as illustrated in Eq. 19. During RCP testing, since NaOH and NaCl solution are enclosed in the testing cell, the energy dissipation to the environment can be omitted. Therefore, all the heat generated due to the electrical current passed is transferred to the solution and result in the temperature increase. Their relationship can be expressed in the form of the heat capacity formula, as shown in Eq. 20.

$$\Delta E = q - W \tag{19}$$

$$m \cdot c \cdot \Delta T = q - 0 \tag{20}$$

Where,

c indicates the specific heat of water, ΔT represents the temperature change during RCP measurements, and m represents the mass of solution used in RCP test.

The mechanism of the previous relationship is that the water solution used in RCP test can be considered a resistor and thus larger the electrical charge caused by the current, higher the temperature increase. Therefore, during the RCP test, a relationship between the extra electrical charge caused by the heating effect and the temperature can be proposed, as shown in Eq. 21.

$$U \cdot (Q - Q_0) = a \cdot m \cdot c \cdot (T - T_0) \tag{21}$$

Where,

U represents the applied voltage (60V) during RCP test, Q_0 is the corrected electrical charge without heating effect, Q is the measured electrical charge after testing, a serves as a correction factor and can be obtained from the fitted curve shown in Fig. 39, T is the temperature at 6 hours, T_0 is the initial temperature.

The corrected total charge value was calculated based on the value of the electrical charge at the first minute during RCP measurement, multiplied by 360 (6h testing time) [33]. There results are plotted in Fig. 39, where x indicates the temperature difference during the test in Celsius and y represents the predicted extra electrical charge in Coulombs caused by heating effect. Therefore,

the correlation between adjusted and measured charge can be established as a function of temperature difference, as shown in Eq. 22. The coefficient of determination value R^2 is 0.8118 which indicates a good fit. For the convenience of evaluating chloride diffusion coefficient, Eq. 23 can be derived from Eq. 17, 18, and 22.

$$Q_0 = Q - 34.07(T - T_0) \tag{22}$$

$$D_i = 0.0236\left[Q - 34.07(T - T_0)\right] \tag{23}$$

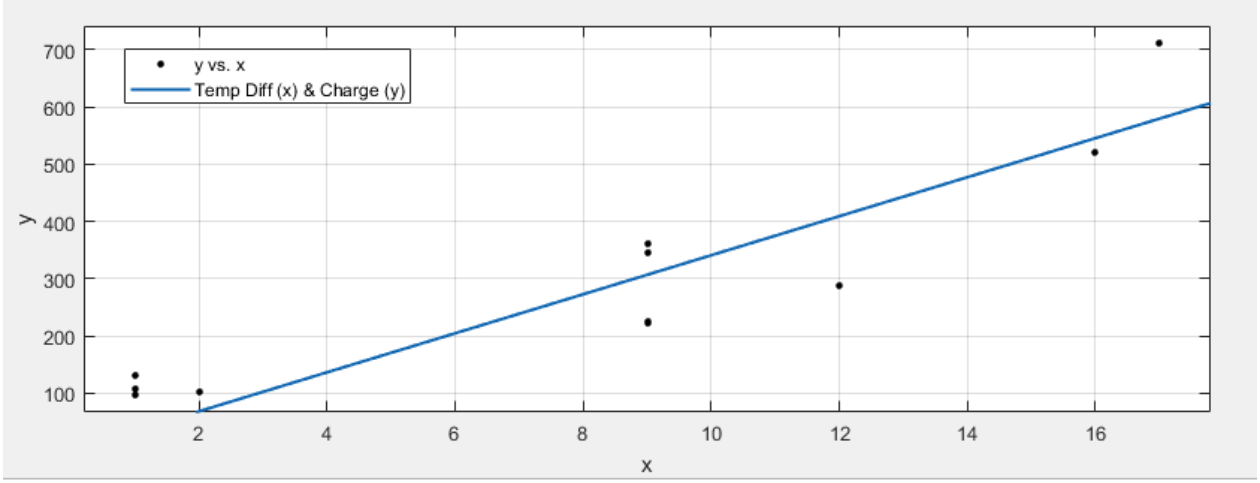

Figure 39 Curve fitting for Eq. 19 based on test data

Model application

In chapter 2, the theoretical relationship between RCP and electrical resistivity methods was discussed, RCP test results did not correlate well with resistivity measurements, as demonstrated in Fig. 25. So, the temperature adjustment model proposed in the previous section can be applied to resolve the problem. Fig. 40 shows the electrical charge of RCP test before and after adjustments using Eq. 22. It can be observed that the adjustment method can bring the results of Mix F and M closer to the theoretical relationship, and because Mix P is closed to theoretical line, the results of Mix P do not change much. However, even after the adjustment, the distance between test results and their theoretical relationship (blue line) is still large. There are several reasons that result in unsatisfied temperature adjustment. Firstly, the model itself is based on limited test results (11 specimens), so regression analysis may not give a good prediction even though R^2 is 0.8118. In

addition, it is widely believed that apart from heating effect, binding effect of repair material to chloride ions and the involvement of supplementary cementitious materials can also deviate the RCP measurements.

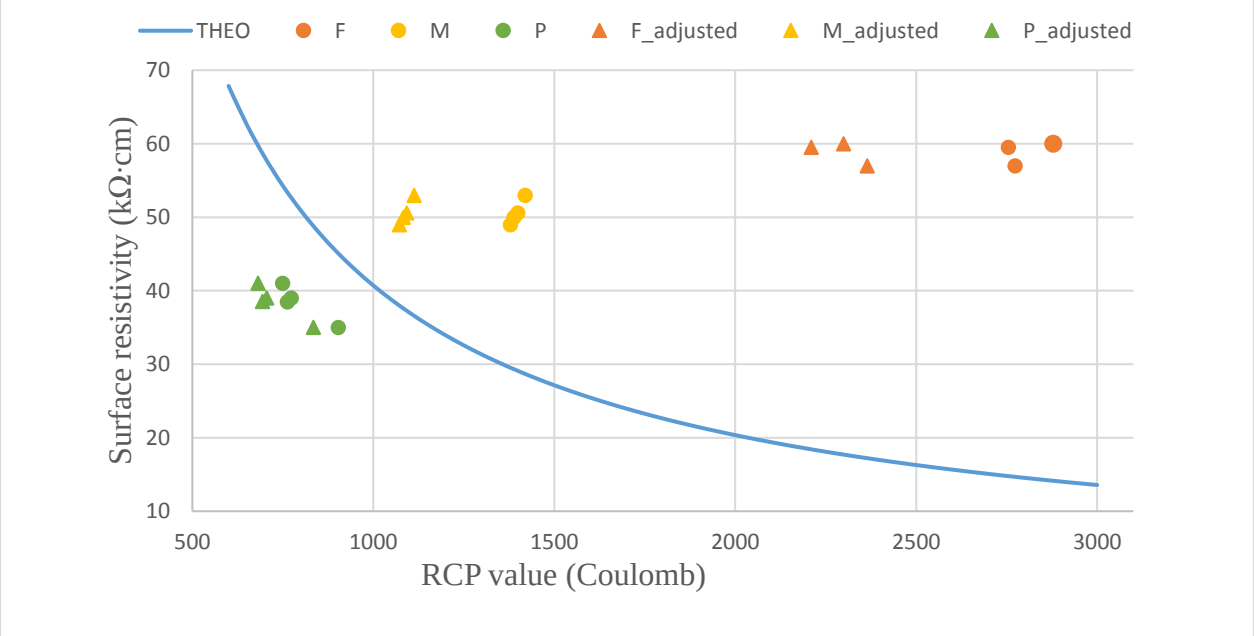

Figure 40 RCP and resistivity relationship after adjustment

Model limitation

The limitation of the using Eq. 22 and Eq. 23 for mitigating temperature effect and for diffusion coefficient calculation is that it may not be applicable in some situations. Firstly, though the regression model shows a high R^2 value, its applicability to repair materials still remains unclear due to the limited number of specimens used in this study. Second, the estimation equation is probably not valid for concrete, which according to ASTM C1202 [32], is classified as having "negligible" or "high" chloride penetrability. The reason lies that there is almost no heating effect if the current passing the specimen is weak, and thus temperature adjustment is not necessary. Whereas, if chloride penetrability is too high, concrete pore structures can also be modified which will not follow our estimation equation. Last, since there are many factors that can deviate RCP results, using a temperature adjustment equation cannot guarantee accurate calculation of chloride diffusion coefficient based on RCP test data. More work is required to build a more comprehensive model taking into account the binding effect and effect of the chemical composition of specimens.

Chapter 5 Conclusion

Based on the experimental study of concrete repair materials using surface/bulk resistivity, RCP, permeability, half-cell potential, compression test and flexural test, the following can be concluded:

a) The surface resistivity method shows a strong correlation with water penetration test, and their relationship can be expressed in the form of a power equation ($R^2 = 0.8573$). Compared with the trendline of conventional concrete, concrete repair material indicates superior resistivity performance at the same water penetration depth.
b) The surface resistivity indicates a linear correlation with bulk resistivity test method ($R^2 = 0.8825$). In our case, the surface resistivity of three repair samples is found to be 2.08 times on average higher than the bulk resistivity, which also supports the finding from other researchers. Therefore, two tests can be used interchangeably to evaluate concrete resistivity performance.
c) Results from RCP test indicate no apparent relationship with concrete resistivity values, which is different than our theoretical predictions. This deviation could be caused by the heating effect due to the high voltage imposed on the testing cell and by the binding effect of concrete, which depends upon its chemical composition.
d) Compressive strength values show a weak correlation to the resistivity properties of repair materials with a coefficient of determination value of only 0.3399. Concrete resistivity is significantly dependent upon the interconnectivity of pores and the conductivity of pore solutions, whereas the compressive strength of concrete is more affected by other factors such as water/cement ratio (w/c), type and amount of cement, weather conditions. However, in our study, material with higher resistivity tends to show high compressive strength. More repair material mixes need to be studied, and the effect of adding supplementary cementitious materials on compression and resistivity also need to be addressed.
e) Half-cell potential measurements did not show any difference in materials with different permeability, compressive strength, and electrical conductance properties. Thus, it is not recommended to evaluate concrete properties based on half-cell potential measurements.

f) Amongst three types of repair materials, cementitious concrete repair (Mix F) shows the highest flexural strength, matrix-rebar bonding strength, and a good energy absorption capability during beam bending process. For fast-setting concrete like Mix P, limited casting time can result in insufficient compaction, and thus bonding strength can be undermined. Therefore, the size of the repair should be strictly limited to attain better repair quality using fast-setting concrete.

g) Compared to cementitious concrete (Mix F) and polymer-modified concrete mortar (Mix P), cementitious concrete mortar (Mix M) show the best durability performance, i.e., low water penetration, high concrete resistivity, and high compressive strength. It is recommended to use water penetration along with surface/bulk electrical tests to evaluate concrete durability.

h) A model is proposed to counteract temperature effect while calculating coefficient of diffusion which indicates the concrete to resist chloride diffusion. It is found that this model can shift the RCP measurement slightly closer to its theoretical prediction but the difference between them is still large. Therefore, further research is required for acquiring more raw data from RCP measurements as the regression analysis input. In addition, a more comprehensive model that involves more correction factors for binding effect, etc., is also needed.

Recommendations for future work

From the previous study, durability indices of three types of repair materials are studied including permeability, electrical resistance, as well as their mechanical properties. There are still some aspects that need more investigations in order to better understand concrete repair materials, provide guidance to industry for repair material selection, and improve the ASTM standard for testing concrete repair materials. The following points are recommended to be considered for future studies:

a) For conducting RCP test on repair materials, the number of the specimen tested should be enlarged. According to ASTM C1202 [32], only one specimen disk can be sliced from 100mm diameter by 200 mm cylinders, which limited the number of specimens in this study. It can be of interest to conduct RCP measurements on the specimens with 1, 3, 7, 28 and 56 days of curing ages and study the electrical charge as a function of specimen ages.

b) The RCP test results can be affected by many factors apart from the heating effect which most researchers mentioned. It is recommended to investigate how much binding effect and the chemical composition of materials can affect RCP results and introduce that part into the adjustment model. Namely, a more compressive model which has more correction factors involved is required.
c) Because the 60-volt DC potential used in RCP test can result in heating effect, it is recommended for ASTM C 1202 to make some adjustments such as using a lower voltage.
d) Due to the fast setting characteristics of repair materials, it is recommended for manufacturers to involve a parameter, which regulates the applicable repair area, in their product specifications. Therefore, poor concrete quality due to insufficient time for compaction can be diminished.
e) Apart from the laboratory study in this research, these three types of repair materials can be applied in real building structures and the comparison can be made in terms of durability performance and compatibility with substrate. Also, rusted rebars can be implanted in repair concrete, and the impediment of repair materials to steel corrosion when corrosion has initiated can also be of interest to study.

Bibliography

[1] "Canadian_Infrastructure_Report_2016.pdf - Google Search." [Online]. Available: http://canadianinfrastructure.ca/downloads/Canadian_Infrastructure_Report_Card_Key_Messages_2016.pdf. [Accessed: 20-Feb-2018].

[2] B. L. Lawrence, "Material selection guideline for structural concrete repair," PhD Thesis, University of Texas at Austin, 1998.

[3] C. S. Suryawanshi, "Structural concrete repair – A durability based revised approach is needed," p. 6.

[4] N. J. R. Baldwin, E. S. King, Great Britain, and Health and Safety Executive, *Field studies of the effectiveness of concrete repairs: phase 1 report : desk study and literature review*. Sudbury: Health and Safety Executive, 2003.

[5] D. R. Morgan, "Compatibility of concrete repair materials and systems," *Constr. Build. Mater.*, vol. 10, no. 1, pp. 57–67, Feb. 1996.

[6] P. H. Emmons and A. M. Vaysburd, "Factors affecting the durability of concrete repair: the contractor's viewpoint," *Constr. Build. Mater.*, vol. 8, no. 1, pp. 5–16, Jan. 1994.

[7] J. P. Broomfield, *Corrosion of Steel in Concrete: Understanding, Investigation and Repair, Second Edition*. CRC Press, 2006.

[8] S. E. Alice, "Selection of High Performance Repair Materials for Pavements and Bridge Decks," PhD Thesis, Cleveland State University, 2014.

[9] A. Vaysburd, "Specifying Concrete Repair Materials," *Mater. Bud.*, vol. 1, no. 3, pp. 44–47, Mar. 2016.

[10] K. D. Stanish, D. Hooton, and M. D. A. Thomas, "Testing the Chloride Penetration Resistance of Concrete: A Literature Review," Jan. 1997.

[11] Q. T. Phung, N. Maes, G. De Schutter, D. Jacques, and G. Ye, "Determination of water permeability of cementitious materials using a controlled constant flow method," *Constr. Build. Mater.*, vol. 47, pp. 1488–1496, Oct. 2013.

[12] *Luftporengehalt von Frischbeton: DIN 1048 ; (Druckausgleichverfahren)*. Horstmann, 1993.

[13] M. G. Alexander, A. Bentur, and S. Mindess, *Durability of concrete: design and construction*. Boca Raton: CRC Press, Taylor & Francis Group, 2017.

[14] J. Tanesi and A. Ardani, "Surface resistivity test evaluation as an indicator of the chloride permeability of concrete," 2012.

[15] "Surface Resistivity as an Alternative for Rapid Chloride... - Google Scholar." [Online]. Available: https://scholar.google.ca/scholar?hl=en&as_sdt=0%2C5&q=Surface+Resistivity+as+an+Alternative+for+Rapid+Chloride+Permeability+Test+of+Hardened+Concrete&btnG=. [Accessed: 20-Feb-2018].

[16] Y. Zhao and W. Jin, *Steel Corrosion-Induced Concrete Cracking*. Butterworth-Heinemann, 2016.

[17] "Fundamentals of Permeability in Asphalt Mixtures - Google Search." [Online]. Available: https://www.google.ca/search?newwindow=1&safe=active&client=firefox-b-ab&dcr=0&ei=T6mLWoDDMMK4jAPBprmwBg&q=Fundamentals+of+Permeability+in+Asphalt+Mixtures&oq=Fundamentals+of+Permeability+in+Asphalt+Mixtures&gs_l=psy-ab.3..0i22i30k1.21229.21229.0.21410.1.1.0.0.0.0.95.95.1.1.0....0...1.1.64.psy-ab..0.1.94....0.BPNDCmyoCUw. [Accessed: 20-Feb-2018].

[18] J. Happel and H. Brenner, *Low Reynolds number hydrodynamics: with special applications to particulate media*. Springer Netherlands, 1983.
[19] G. W. Scherer, J. J. Valenza, and G. Simmons, "New methods to measure liquid permeability in porous materials," *Cem. Concr. Res.*, vol. 37, no. 3, pp. 386–397, Mar. 2007.
[20] M. Ibrahim and M. Issa, "Evaluation of chloride and water penetration in concrete with cement containing limestone and IPA," *Constr. Build. Mater.*, vol. 129, pp. 278–288, Dec. 2016.
[21] Jones Christopher A. and Grasley Zachary C., "Correlation of Radial Flow-Through and Hollow Cylinder Dynamic Pressurization Test for Measuring Permeability," *J. Mater. Civ. Eng.*, vol. 21, no. 10, pp. 594–600, Oct. 2009.
[22] A. Bhargava and N. Banthia, "Measurement of Concrete Permeability Under Stress," *Exp. Tech.*, vol. 30, no. 5, pp. 28–31, Sep. 2006.
[23] J. R. Nimmo, J. Rubin, and D. P. Hammermeister, "Unsaturated flow in a centrifugal field: Measurement of hydraulic conductivity and testing of Darcy's Law," *Water Resour. Res.*, vol. 23, no. 1, pp. 124–134, Jan. 1987.
[24] A. S. El-Dieb and R. D. Hooton, "Water-permeability measurement of high performance concrete using a high-pressure triaxial cell," *Cem. Concr. Res.*, vol. 25, no. 6, pp. 1199–1208, Aug. 1995.
[25] "A high pressure triaxial cell with improved measurement sensitivity for saturated water permeability of high performance concrete - ScienceDirect." [Online]. Available: https://www-sciencedirect-com.ezproxy.library.uvic.ca/science/article/pii/0008884694900051. [Accessed: 20-Feb-2018].
[26] C. A. Jones and Z. C. Grasley, "Correlation of hollow and solid cylinder dynamic pressurization tests for measuring permeability," *Cem. Concr. Res.*, vol. 39, no. 4, pp. 345–352, Apr. 2009.
[27] G. W. Scherer, "Measuring Permeability of Rigid Materials by a Beam-Bending Method: I, Theory," *J. Am. Ceram. Soc.*, vol. 83, no. 9, pp. 2231–2239, Sep. 2000.
[28] W. Vichit-Vadakan and G. W. Scherer, "Measuring Permeability of Rigid Materials by a Beam-Bending Method: II, Porous Glass," *J. Am. Ceram. Soc.*, vol. 83, no. 9, pp. 2240–2246, Sep. 2000.
[29] G. W. Scherer, "Thermal Expansion Kinetics: Method to Measure Permeability of Cementitious Materials: I, Theory," *J. Am. Ceram. Soc.*, vol. 83, no. 11, pp. 2753–2761, Nov. 2000.
[30] G. W. Scherer, H. Hdach, and J. Phalippou, "Thermal expansion of gels: a novel method for measuring permeability," *J. Non-Cryst. Solids*, vol. 130, no. 2, pp. 157–170, Jul. 1991.
[31] D. Whiting, "RAPID MEASUREMENT OF THE CHLORIDE PERMEABILITY OF CONCRETE," *Public Roads*, vol. 45, no. 3, Dec. 1981.
[32] "ASTM C1202-17a, Standard Test Method for Electrical Indication of Concrete's Ability to Resist Chloride Ion Penetration, ASTM International, West Conshohocken, PA, 2017, www.astm.org." .
[33] G. A. Julio-Betancourt and R. D. Hooton, "Study of the Joule effect on rapid chloride permeability values and evaluation of related electrical properties of concretes," *Cem. Concr. Res.*, vol. 34, no. 6, pp. 1007–1015, Jun. 2004.
[34] H. Layssi, P. Ghods, A. R. Alizadeh, and M. Salehi, "Electrical resistivity of concrete," *Concr. Int.*, vol. 37, no. 5, pp. 41–46, 2015.

[35] H. A. F. Dehwah, “Durability of reinforced concrete beams repaired with various repair materials,” PhD Thesis, KFUPM, 1990.
[36] M. M. Al-Zahrani, M. Maslehuddin, S. U. Al-Dulaijan, and M. Ibrahim, “Mechanical properties and durability characteristics of polymer- and cement-based repair materials,” *Cem. Concr. Compos.*, vol. 25, no. 4, pp. 527–537, May 2003.
[37] M. Luković, G. Ye, and K. Van Breugel, “Reliable concrete repair-a critical review,” in *Proc. of international conference Structural Faults & Repair*, 2012.
[38] A. Saccani and V. Magnaghi, “Durability of epoxy resin-based materials for the repair of damaged cementitious composites,” *Cem. Concr. Res.*, vol. 29, no. 1, pp. 95–98, Jan. 1999.
[39] M. El-Hawary, H. Al-Khaiat, and S. Fereig, “Performance of epoxy-repaired concrete in a marine environment,” *Cem. Concr. Res.*, vol. 30, no. 2, pp. 259–266, Feb. 2000.
[40] J. Cabrera and A. Al-Hasan, “Performance properties of concrete repair materials,” *Constr. Build. Mater.*, vol. 11, no. 5, pp. 283–290, Jan. 1997.
[41] P. S. Mangat and M. K. Limbachiya, “Repair material properties which influence long-term performance of concrete structures,” *Constr. Build. Mater.*, vol. 9, no. 2, pp. 81–90, Apr. 1995.
[42] H. Ueda, Y. Tamai, and T. Kudo, “Evaluation of the Durability of Cement-based Repair Materials,” *Q. Rep. RTRI*, vol. 52, no. 2, pp. 92–96, 2011.
[43] J. Wongpa, K. Kiattikomol, C. Jaturapitakkul, and P. Chindaprasirt, “Compressive strength, modulus of elasticity, and water permeability of inorganic polymer concrete,” *Mater. Des.*, vol. 31, no. 10, pp. 4748–4754, Dec. 2010.
[44] N. Hearn, “Saturated permeability of concrete as influenced by cracking and self-sealing.,” PhD Thesis, University of Cambridge, 1993.
[45] P. A. Snehal and D. B. Shekhar, “Electrical Properties And Compressive Strength of Concrete With SCMs and COIRS,” *International Journal of Advanced Technology in Civil Engineering*, vol. 1, no. 2, pp. 119–121, 2012.
[46] A. Lübeck, A. L. G. Gastaldini, D. S. Barin, and H. C. Siqueira, “Compressive strength and electrical properties of concrete with white Portland cement and blast-furnace slag,” *Cem. Concr. Compos.*, vol. 34, no. 3, pp. 392–399, Mar. 2012.
[47] A. A. Ramezanianpour, A. Pilvar, M. Mahdikhani, and F. Moodi, “Practical evaluation of relationship between concrete resistivity, water penetration, rapid chloride penetration and compressive strength,” *Constr. Build. Mater.*, vol. 25, no. 5, pp. 2472–2479, May 2011.
[48] P. Ghosh and Q. Tran, “Correlation Between Bulk and Surface Resistivity of Concrete,” *Int. J. Concr. Struct. Mater.*, vol. 9, no. 1, pp. 119–132, Mar. 2015.
[49] “ASTM C192 / C192M-16a, Standard Practice for Making and Curing Concrete Test Specimens in the Laboratory, ASTM International, West Conshohocken, PA, 2016, www.astm.org.”
[50] “ASTM C31 / C31M-18, Standard Practice for Making and Curing Concrete Test Specimens in the Field, ASTM International, West Conshohocken, PA, 2018, www.astm.org.”
[51] C. ASTM, “39, Standard test method for compressive strength of cylindrical concrete specimens,” *ASTM Int.*, 2001.
[52] “Strain Gage Installations for Concrete Structures - Tech Tip pdf - Google Search.” [Online]. Available: https://www.google.ca/search?newwindow=1&safe=active&client=firefox-b-ab&dcr=0&ei=aXKQWuixK4bd0gLei6OQAQ&q=Strain+Gage+Installations+for+Concrete+Structures+-+Tech+Tip+pdf&oq=Strain+Gage+Installations+for+Concrete+Structures+-

+Tech+Tip+pdf&gs_l=psy-ab.3...6141.7458.0.7601.4.4.0.0.0.0.98.276.4.4.0....0...1.1.64.psy-ab..0.0.0....0.mpBdCC5bA74. [Accessed: 23-Feb-2018].
[53] "ASTM C293 / C293M-16, Standard Test Method for Flexural Strength of Concrete (Using Simple Beam With Center-Point Loading), ASTM International, West Conshohocken, PA, 2016, www.astm.org."
[54] "AASHTO TP 95 - Standard Method of Test for Surface Resistivity Indication of Concrete's Ability to Resist Chloride Ion Penetration | Engineering360." [Online]. Available: https://standards.globalspec.com/std/9863485/aashto-tp-95. [Accessed: 30-Apr-2018].
[55] M. Ibrahim and M. Issa, "Evaluation of chloride and water penetration in concrete with cement containing limestone and IPA," *Constr. Build. Mater.*, vol. 129, no. Supplement C, pp. 278–288, Dec. 2016.
[56] "ASTM C876-15, Standard Test Method for Corrosion Potentials of Uncoated Reinforcing Steel in Concrete, ASTM International, West Conshohocken, PA, 2015, www.astm.org."
[57] X. Shi, L. Fay, M. M. Peterson, M. Berry, and M. Mooney, "A FESEM/EDX investigation into how continuous deicer exposure affects the chemistry of Portland cement concrete," *Constr. Build. Mater.*, vol. 25, no. 2, pp. 957–966, Feb. 2011.
[58] S. Mindess, J. F. Young, and D. Darwin, *Concrete*, 2nd ed. Upper Saddle River, NJ: Prentice Hall, 2003.
[59] "Probabilistic risk assessment," *Wikipedia*. 01-Apr-2018.
[60] Q. Yuan, C. Shi, G. De Schutter, K. Audenaert, and D. Deng, "Chloride binding of cement-based materials subjected to external chloride environment – A review," *Constr. Build. Mater.*, vol. 23, no. 1, pp. 1–13, Jan. 2009.
[61] M. D. A. Thomas, R. D. Hooton, A. Scott, and H. Zibara, "The effect of supplementary cementitious materials on chloride binding in hardened cement paste," *Cem. Concr. Res.*, vol. 42, no. 1, pp. 1–7, Jan. 2012.
[62] "ASTM C150 / C150M-18, Standard Specification for Portland Cement, ASTM International, West Conshohocken, PA, 2018, www.astm.org."
[63] R. P. Spragg, J. Castro, T. Nantung, M. Paredes, and J. Weiss, "Variability analysis of the bulk resistivity measured using concrete cylinders," *Adv. Civ. Eng. Mater.*, vol. 1, no. 1, pp. 1–17, 2012.
[64] J. Gudimettla and G. Crawford, "Resistivity Tests for Concrete–Recent Field Experience.," *ACI Mater. J.*, vol. 113, no. 4, 2016.
[65] P. Azarsa and R. Gupta, "Electrical Resistivity of Concrete for Durability Evaluation: A Review," *Advances in Materials Science and Engineering*, 2017. [Online]. Available: https://www.hindawi.com/journals/amse/2017/8453095/. [Accessed: 21-Jan-2018].
[66] A. Noushini, B. Samali, and K. Vessalas, *Flexural Toughness and Ductility Characteristics of Polyvinyl-Alcohol Fibre Reinforced Concrete (PVA-FRC)*. International Center for Numerical Methods in Engineering (CIMNE), 2013.
[67] P. Robins, S. Austin, and P. Jones, "Pull-out behaviour of hooked steel fibres," *Mater. Struct.*, vol. 35, no. 7, pp. 434–442, Aug. 2002.
[68] M. J. Shannag, R. Brincker, and W. Hansen, "Pullout behavior of steel fibers from cement-based composites," *Cem. Concr. Res.*, vol. 27, no. 6, pp. 925–936, Jun. 1997.
[69] J. Lizarazo-Marriaga and P. Claisse, "Modelling chloride penetration in concrete using electrical voltage and current approaches," *Mater. Res.*, vol. 14, no. 1, pp. 31–38, Mar. 2011.
[70] "First law of thermodynamics," *Wikipedia*. 15-Apr-2018.

Appendix A Material and Equipment Specifications

Materials

TARGET Flowcrete is one type of cementitious concrete repair and termed as Mix F in the context of our discussion. Data sheet provided by the supplier is shown below:

TYPICAL PROPERTIES OF TARGET FLOWCRETE WITH 5% SILICA FUME

MIX CONSISTENCY	FLOWABLE	PLASTIC
WATER ADDED Litres / 25 kg bag (US gallons) / 55 lb bag	 2.5 – 2.6 (.66 - .687)	 2.2 – 2.3 (.58 - .61)
RAPID CHLORIDE PERMEABILITY (ASTM C1202; 56 Day Cycle)	365 (Very Low)	
SLUMP, mm (inches) CSA A23.2-5C	180-220 (7-9)	100-130 (4-5)
FLOW, cm (in) DIN EN 12350-5	60(23.6)	Not Applicable
COMPRESSIVE STRENGTH MPa (lb/in^2) ASTM C109 (CSA A23.2-3C,9C) 100mm diameter cylinders at 1 day at 7 days at 28 days	 16 (2350) 37 (5400) 45 (6500)	 24 (3500) 48 (7000) 55 (8000)
VOLUME CHANGE % expansion Prior to initial set, unrestrained, CSA A23.2-1B After final set, CRD-C621 at 3 days at 7 days at 28 days	 0 0.02 0.02 0.02	 0 0.01 0.01 0.01
AIR CONTENT, % volume CSA A23.2-4C	 5.8	 5.1

MasterEmaco T430 is one type of cementitious concrete repair mortar and termed as Mix M in the context of our discussion. Data sheet provided by the supplier is shown below:

Test Data[1]

PROPERTY	RESULTS			TEST METHOD
Compressive strength, psi (MPa), at 70° F (21° C)				ASTM C 109
3 hrs	1,000 (7)			
24 hrs	4,500 (31)			
7 days	7,800 (54)			
28 days	9,000 (62)			
Setting time, min				ASTM C 266 at 72° F (22° C)
	50° F (10° C)	**70° F (21° C)**	**90° F (32° C)**	
Initial set	140	75	65	
Final set	160	90	75	
	1 Day Psi (MPa)	**7 Day Psi (MPa)**	**28 Day Psi (MPa)**	
Flexural strength	580 (4.0)	880 (6.1)	1,150 (7.9)	ASTM C 348
Splitting tensile	550 (3.8)	1,100 (7.6)	1,250 (8.6)	ASTM C 496
Slant shear bond	1,800 (12.4)	3,000 (20.7)	3,360 (23.2)	ASTM C 882
Direct shear bond	150 (1.0)	390 (2.7)	450 (3.1)	Michigan DOT
Direct tensile bond	100 (0.7)	170 (1.2)	290 (2.0)	BASF method
Modulus of elasticity, psi (GPa)	5.1×10^6 (35)			
Abrasion resistance, in (cm) of wear, 28-day, air-cured sample				ASTM C 779 A
30 min	0.0120 (0.0305)			
60 min	0.0240 (0.0610)			
Freeze/thaw resistance, % RDM	98.5			ASTM C 666 A
Rapid chloride permeability[2], coulombs	990 (very low)			AASHTO-T277 / ASTM C 1202
Scaling resistance, weight loss, lb/ft²				ASTM C 672
25 cycles	$CaCl_2$: 0.003	NaCl: 0.067		
50 cycles	$CaCl_2$: 0.005	NaCl: 0.084		

[1]Typical results from air cured samples.
[2]Typical results from 3 days moist-cured and 39 days air-cured samples.
Results were obtained when material was mixed with 0.52 gallons (2 L) of water per bag and cured at 72° F (22° C). Expect reasonable variations, depending upon mixing equipment, temperature, application methods, test methods, and curing conditions.

MAIPEI PlanitopX is one type of polymer-modified repair mortar and termed as Mix P in the context of our discussion. Data sheet provided by the supplier is shown below:

Product Performance Properties*

Laboratory Tests	Results
Compressive strength – ASTM C109 (CAN/CSA-A5)	
3 hours	> 3,800 psi (26,2 MPa)
1 day	> 5,600 psi (38,6 MPa)
7 days	> 6,650 psi (45,9 MPa)
28 days	> 7,300 psi (50,3 MPa)
Flexural strength – ASTM C348 (CAN/CSA-A23.2-8C)	
1 day	> 1,000 psi (6,90 MPa)
7 days	> 1,200 psi (8,28 MPa)
28 days	> 1,450 psi (10 MPa)
Tensile bond strength – ASTM C1583 (CSA CAN/A23.2-6B) (failure in concrete substrate)	
28 days	> 290 psi (2 MPa)
Slant/shear bond strength – ASTM C882 (modified)	
1 day	> 1,400 psi (9,66 MPa)
28 days	> 1,880 psi (13,0 MPa)
Volume change – Meets ASTM C928 requirements	
28 days, dry-cured	< -0.15%
28 days, wet-cured	< +0.15%

** All tests were performed at 73°F (23°C) and 50% relative humidity with a mixture of 1 U.S. gal. (3,79 L) of water per 50-lb. (22,7-kg) bag of* Planitop X. *An increase in the water content will alter listed properties.*

Appendix B Flexural strength/toughness/strain

The following tables contain the flexural response of repair materials tested in this study including flexural strength, toughness, and strain. Tests were performed on 6'' by 6'' by 21'' prismatic specimens cured at ambient and elevated temperature which is detailed in Table 6.

Flexural properties

Mix	Specimen#	Flexural strength	Flexural toughness	Maximum strain on rebar
F	1	9.47	62113.63	n/a
	2	10.25	n/a	0.001932
	3	11	76514.89	n/a
	4	11.84	43703.24	0.003522
	5	11.27	52656.76	0.002317
	6	10.76	71420.45	n/a
	7	10.28	66965.06	0.002432
M	1	9.11	n/a	0.002369
	2	11.016	23246.73	0.002392
	3	8.79	n/a	n/a
	4	9.51	62510.45	n/a
	5	10.04	43914.91	0.002515
P	1	9.05	52319.61	n/a
	2	10.28	101296.89	n/a
	3	8.81	n/a	n/a
	4	9.90	73761.82	n/a
	5	11.12	31436.19	n/a
	6	10.41	81875.63	0.001602
	7	10.04	48303.45	0.001654
	8	7.92	46396.81	0.001108